Hindawi
Shock and Vibration
Volume 2019, Article ID 8528763, 23 pages
https://doi.org/10.1155/2019/8528763

Research Article

Data-Driven Synchronization Analysis of a Bouncing Crowd

Jun Chen[1,2] **Huan Tan**[2] **Katrien Van Nimmen**[3,4] **and Peter Van den Broeck**[3,4]

[1]*College of Civil Engineering and Architecture, Xinjiang University, Ürümqi 830047, China*
[2]*College of Civil Engineering, Tongji University, Siping Road No. 1239, Shanghai 200092, China*
[3]*KU Leuven, Department of Civil Engineering, Structural Mechanics, B-3001 Leuven, Belgium*
[4]*KU Leuven, Department of Civil Engineering, Technology Cluster Construction, Structural Mechanics, B-9000 Ghent, Belgium*

Correspondence should be addressed to Jun Chen; cejchen@tongji.edu.cn

Received 6 January 2019; Accepted 1 April 2019; Published 11 June 2019

Academic Editor: Stefano Manzoni

Vibration serviceability problems concerning lightweight, flexible long-span floors and cantilever structures such as grandstands generally arise from crowd-induced loading, in particular due to bouncing or jumping activities. Predicting the dynamic responses of these structures induced by bouncing and jumping crowds has therefore become a critical aspect of vibration serviceability design. Although accurate models describing the load induced by a single person are available, essential information on the level of synchronization within the crowd is missing. In answer to this lack of information, this paper experimentally investigates the inter- and intraperson variability as well as the global crowd behavior in bouncing crowds. A group size of 48 persons is considered in the experiment whereby the individual body motions are registered synchronously by means of a 3D motion capture system. Preliminary tests verified a new approach to characterize the bouncing motion via markers on the clavicle. Subsequently, the full-scale experimental study considered various crowd spacing parameters, auditory stimuli, and bouncing frequencies. Moreover, special test cases were performed whereby each participant was wearing an eyepatch to exclude visual effects. Through the analysis of 330 test cases, the interperson variability at the bouncing frequency is identified. In addition, the cross-correlation and coherence between participants are analyzed. The coherence coefficients between each pair of participants in the same row or column are calculated and can be described by a lognormal distribution function. The influence of the spatial configurations and visual and auditory stimuli is analyzed. For the considered spatial configurations, no relevant impact on the inter- and intraperson variability in the bouncing motion nor in the global crowd behavior is observed. Visual stimuli are found to enhance the coordination and synchronization. Without eyesight, the participants are feeling uncertain about their bouncing behavior. The results evaluating the auditory cues indicate that significantly higher levels of synchronization and a lower degree of the intraperson variability are attained when a metronome cue is used in comparison to songs where the tempo often varies.

1. Introduction

Due to their slenderness, long-span floors and cantilever grandstand structures are very often prone to crowd-induced vibrations [1]. Evaluating the vibration serviceability under crowd-induced rhythmic loading has become a critical aspect of the structural design process. This is particularly relevant for structures such as grandstands used for pop/rock concerts or sporting events as well as the long-span floors accommodating gym and aerobic activities. When the crowd follows a musical beat or an auditory cue with a specific rhythm, the (near) resonant excitation can induce high structural vibration levels [2]. When the vibration levels are too high or when structural movement is alarming, vibration comfort cannot be ensured, and the crowd safety may be at risk [3].

In many cases, crowds may find bouncing preferable over jumping due to the lower energy requirements [1]. Therefore, bouncing represents the primary form of body synchronization when people listen to music during, for example, a concert [4]. Extensive research has been performed to provide a reliable and practical Fourier series representation of the individual bouncing load by measuring the continuous ground reaction forces (GRFs) via force

plates [5–7]. An acceleration response spectrum method has also been developed to calculate structural responses due to individual bouncing [8]. Although essential in the vibration serviceability assessment, no or little information is available involving the levels of synchronization than can be expected within a bouncing crowd. Mouring [9] and Brownjohn et al. [10] agreed that quantification of the degree of correlation between people in a crowd is a primary task for future research. This lack of knowledge on the synchronization behavior of bouncing crowds was the key motivation for this work.

It has been observed that the stimuli of visual, auditory (metronome and music songs), and tactile cues often have a significant impact upon the mutual interaction of bouncing and jumping persons [11–14]. Noormohammadi et al. [12] studied the effect of an auditory metronome as well as visual and tactile stimuli on the level of synchronization between two jumping or bouncing persons using force plates and a motion capture system. Their research also showed that the highest level of synchronization is attained with the auditory metronome [12]. In the second and third place are the visual and tactile stimuli, respectively. Also using a CODA system, Vitomir et al. [13] investigated the effect of the position and proximity between two bouncing bodies on the resulting level of synchronization. It was observed that pairs are best synchronized when facing each other and holding hands. Georgiou et al. [14] used force plates to obtain the force signals of 15 participants to a selection of popular pop and rock songs with different dominant beats [15]. In this research, no strong synchronization pattern between individuals in the group was observed. The highest, yet only moderate, level of synchronization was obtained for songs with predominant beats in the 2-3 Hz range. When the structural response to bouncing is of interest, it is important to also consider the biodynamic parameters of the human body like mass, damping, and stiffness [16–18]. These biodynamic parameters fall outside the scope of this paper and are therefore not further considered here.

Up to now, only a limited number of people (max. 15) were considered in crowd-bouncing experiments [11–15]. The use of force plates to measure large groups ($N > 15$) of bouncing persons is impractical due to the complicated experimental setup and the related high experimental cost. Recently, other experimental approaches that are primarily developed for application in biomechanical sciences are being adopted to investigate human-induced loads, such as the optical marker-based technology of Vicon [19], CODA [20], and the 3D inertial motion-tracking techniques for the registration of in-field pedestrian behavior [21]. Cappozzo et al. [22] explained the theory of the reconstruction of the body motion using the motion capture system with target markers stuck to the skin surface of the participant. The markers were placed in a manner to satisfy technical requirements, such as optimal visibility of the markers in the crowd and minimal relative displacement between the markers and the underlying bone. The key advantage and novelty of using a motion capture system is the feasibility to measure individual characteristics of each person in the crowd simultaneously, which makes it possible to analyze the interaction and correlation between the participants.

Considering the need for information on the synchronization behavior of bouncing crowds, this study presents an extensive experimental study involving the bouncing activity of 48 persons. The individual body motion of each participant was tracked using an optical marker-based technology. A novel approach to crowd-bouncing analysis is based on the trajectory of the clavicle and its new role in characterizing the bouncing motion of a person. Next, up to 330 test cases are performed and analyzed to determine the influence of various factors such as density, sound, or visual stimuli on the behavior of the individual and the crowd.

The outline of this paper is as follows: First, the experimental method is verified using small-scale laboratory experiments and the large-scale experimental study is presented in Section 2. Section 3 introduces methods to analyze intra- and interperson variability and to assess the participant level of synchronization in the test group as it relates to a crowd scenario. Finally, Section 4 analyzes the influence of various stimuli. Conclusions are drawn in Section 5.

2. Crowd-Bouncing Experiments by Motion Capture Technique

In this section, the verification of the applied experimental method and the large-scale experimental study are described. First, Section 2.1 shows that the trajectories of the markers on the clavicle can reliably represent an individual bouncing motion. Second, Section 2.2 describes the experimental setup and test cases conducted.

2.1. Verification of the Experimental Method. Experience from individual tests using the motion capture technique [23] shows that markers need to be placed on locations that are close to the center of mass (COM) of the human body, e.g., bone joints close to the pelvis. When many participants are involved, however, it is impossible to capture the trajectories of markers attached to all major bone joints or close to the center of mass because these markers are easily visually obstructed by adjacent participants in the crowd. Therefore, the verification test investigated if the trajectory of a marker on the clavicle can characterize the bouncing motion of the body. All tests were conducted in the gait analysis laboratory of Shuguang Hospital, Shanghai, China, which is equipped with an advanced Vicon motion capture system [24] and four force plates embedded in the floor at the floor level (Figure 1). The size of a single force platform in Figure 1 is 464×508 mm. The bouncing person therefore has no concern on stepping outside the edge of the platform or falling down. The participants therefore did not have to modify their behavior to ensure full contact with the force plate. The motion capture system consists of 12 infrared cameras and allows for synchronous recording of the

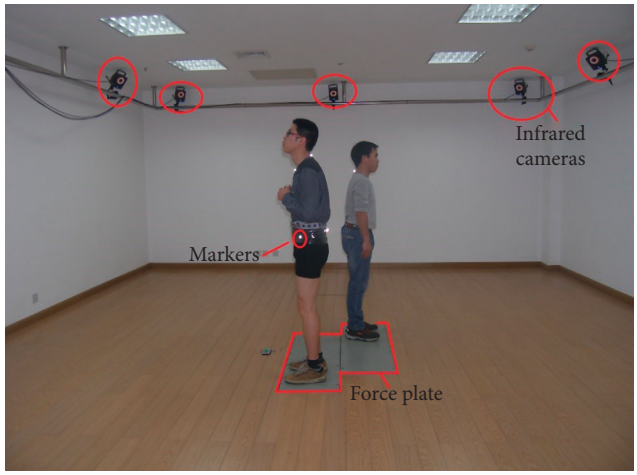

Figure 1: Gait analysis laboratory of Shuguang Hospital.

motion of the reflective markers. The measurement accuracy of the system is 0.1 mm. More information about the motion capture technology can be found in the study by Peng et al. [24]. The applied sampling rate was 1000 Hz for the force plates and 100 Hz for the motion capture system. The force plate was instrumented to measure lateral, longitudinal, and vertical components simultaneously. In this paper, only the vertical component of force was used as this is the dominant component of the bouncing load. In the verification test, two participants were standing on separate force plates and were requested to bounce at four metronome frequencies f_m (2.0, 2.5, 3.0, and 3.5 Hz). The bouncing force of each participant was recorded by the force plate during the test. Each participant was equipped with three markers attached to the clavicle and four markers attached to the pelvis. The average trajectory (typically presented in terms of acceleration) of the four markers close to the pelvis is known as an excellent approximation of the trajectory of the COM, also shown by Zhang et al. [23]. Thus, it is later referred to as COM acceleration. Similarly, the average value of the markers on the clavicle was calculated and taken as the representative acceleration of the clavicle.

A jumping person is usually simplified as a single rigid segment during the reproduction of jumping load via his trajectory of center of mass. However, a bouncing person that remains with two feet on the ground cannot be simplified in a similar way because not his full body mass participates in the bouncing motion. For example, the feet do not (or barely) move during the bouncing motion. Similar observations are made for walking [25, 26]. It is outside the scope of this paper to biomechanically identify the mass distribution and activated mass of the person during the dynamic bouncing motion. As in [27, 28], R ($0 < R \leq 1$) is defined as a dynamic participation coefficient which is the ratio of that part of the effective mass participating in body motion and the whole human mass.

Then, an equivalent vertical acceleration can be determined using the measured bouncing force by the following equation:

$$\ddot{u}_{\text{equ}}(t) = \frac{F_v(t) - mg}{mR}, \tag{1}$$

where $\ddot{u}_{\text{equ}}(t)$ (m/s^2) represents the equivalent vertical acceleration of the body's COM, $F_v(t)$ (N) is the vertical bouncing force measured by the force plate, m (kg) is the body mass, and g is the gravity acceleration. The R coefficient is dependent on the BMI (body mass index) of the participant and the bouncing frequency. The R values at one frequency in this paper were the average of individual R values that were estimated by trial and error to minimize the difference of the RMS of one's clavicle and the equivalent acceleration time histories. The values of R adopted in this study are summarized in Table 1. They were determined by the empirical approach described in [28].

Figure 2 compares time histories of the COM, clavicle, and equivalent acceleration from one test case. The comparison shows that the three curves are very similar to each other. This observation stands for other test cases, indicating that the trajectory of the clavicle can be used to represent motion of COM of a bouncing person. The results in Table 1 show that the ratios of peaks of the clavicle acceleration and the equivalent acceleration derived from the force with R taken into account are in close agreement. Note that the ratios are very close to 1.0, implying that the two accelerations have nearly the same amplitude. Table 2 further shows the linear correlation coefficients between the clavicle and equivalent acceleration from all test cases. The high correlation values, which are all larger than 0.98, indicate clearly high similarity between the two accelerations in global sense. The verification experiments prove that the trajectory of the clavicle can represent the characteristic of the bouncing force. Therefore, when trajectories of all persons in a crowd can be monitored simultaneously, they can be used to explore the synchronization between bouncing persons.

2.2. Crowd-Bouncing Experiment. The experimental study on crowd bouncing was carried out in the Civil Engineering Building of Tongji University, and all participants were students. The test protocol satisfied the requirements by the Tongji Medical Ethics Committee. The experiments were conducted using a Vicon motion capture system consisting of 18 infrared cameras (Figure 3), and a sample rate of 100 Hz was applied. The tests considered 48 persons standing in a 6×8 matrix configuration with each participant equipped with three markers on his/her clavicle (Figure 4). Each participant was labelled with a number from 1 to 48 according to their position in the matrix setup. To examine the effects of various parameters on the level of synchronization in crowd bouncing on a rigid floor, bouncing tests were carried out considering different metronome rhythms, songs, and spatial distribution, with or without obstructing the view of the participants using eyepatches. The specifications of the tests are listed in Table 3. The tests were repeated on three different days, involving different participants: 84 males (age: 21.9 ± 2.5 yrs; weight: 65.03 ± 7.95 kg; height: 1.74 ± 0.058 m (mean $\pm$ standard deviation)) and 47 females (age: 22.4 ± 2.3 yrs;

Table 1: Mean values and standard deviation of the ratio of peaks of the clavicle acceleration and the equivalent acceleration (—).

Frequency (Hz)	2.0 ($R = 0.8$)		2.5 ($R = 0.77$)		3.0 ($R = 0.75$)		3.5 ($R = 0.73$)	
	μ	σ	μ	σ	μ	σ	μ	σ
Participant 1	1.032	0.035	1.091	0.037	1.032	0.035	1.091	0.037
Participant 2	1.002	0.036	0.967	0.058	1.002	0.036	0.967	0.058

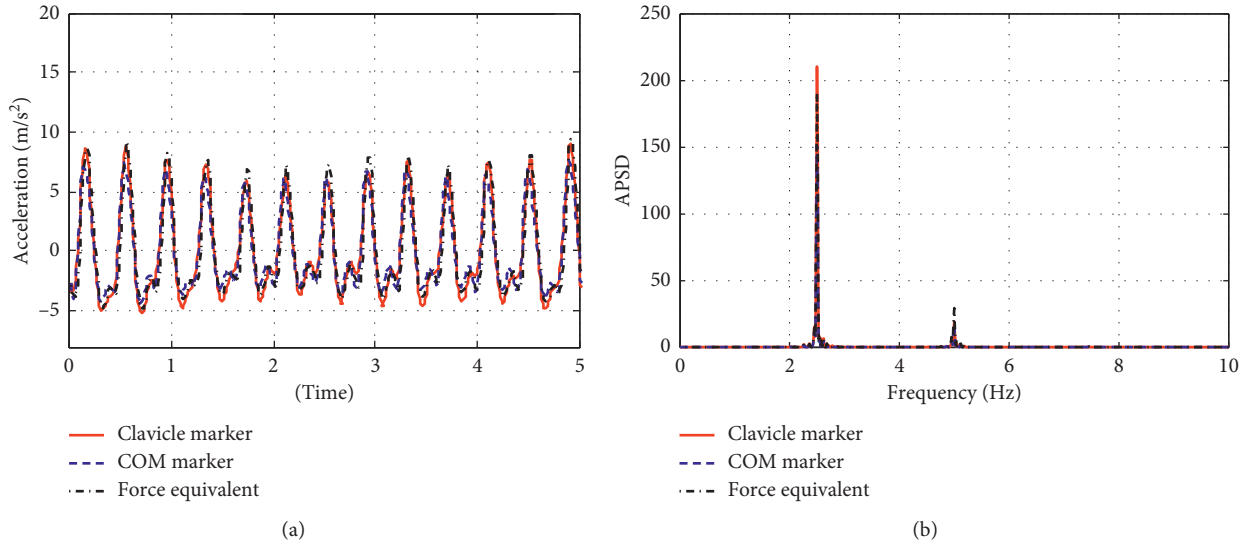

Figure 2: Comparison of the time histories of the accelerations corresponding to the clavicle, the COM, and the equivalent acceleration considering a metronome frequency of 2.5 Hz. (a) Time histories; (b) autopower spectral density.

Table 2: Correlation values between the clavicle acceleration and equivalent acceleration.

Frequency (Hz)	2.0	2.0	2.0	2.5	2.5	3.0	3.0	3.5	3.5	3.5
Participant 1	0.995	0.994	0.995	0.995	0.996	0.993	0.994	0.989	0.989	0.983
Participant 2	0.990	0.994	0.993	0.988	0.985	0.993	0.992	0.987	0.988	0.983

Figure 3: Experimental setup involving 18 high-speed infrared cameras.

Figure 4: Forty-eight participants standing in the reference configuration.

weight: 52.35 ± 4.85 kg; height: 1.63 ± 0.041 m (mean ± standard deviation)).

Table 3 lists the specifications of all tests that were considered on each test day. Extensive experiments were arranged for the 1 m × 1 m (front to back × left to right) spacing configuration which is considered in this study as the *reference configuration/density*. Specifically, 32 test cases were conducted under various audio cues: 21 metronome-guided frequencies from 1.5 to 3.5 Hz with an interval of 0.1 Hz and eight pop songs. The metronome frequencies

Table 3: Specification of the performed tests.

Parameters	Specifications		
Spacing (m)*	1×1	1×1	1×0.8; 1×0.6; 0.8×1; 1.2×1; 0.8×0.6
Metronome frequency (Hz)	1.5 to 3.5 ($\Delta f = 0.1$)	1.5 to 3.5 ($\Delta f = 0.1$)	1.5 to 3.5 ($\Delta f = 0.5$)
Eyepatch	Without	With	Without
Music	11 songs	11 songs	8 songs

*Front-back × left-right.

were randomized in successive tests to avoid "habituation" of test subjects, thereby adjusting their performance to monotonously increasing or decreasing beats. Each test case was repeated twice (denoted as rounds 1 and 2 hereafter) on every test day leading to a total of 192 test cases. Additional tests with participants wearing an eyepatch were conducted for 21 metronome-guided frequencies and 11 songs. To investigate the effect of crowd density, five other spacing configurations were considered in the experiment, which are $1\,\text{m} \times 0.8\,\text{m}$, $1\,\text{m} \times 0.6\,\text{m}$, $0.8\,\text{m} \times 1\,\text{m}$, $1.2\,\text{m} \times 1\,\text{m}$, and $0.8\,\text{m} \times 0.6\,\text{m}$. For each of the five configurations, 13 test cases, all without eyepatch, were conducted, in which 5 are metronome-guided cases (1.5 to 3.5 Hz with an interval of 0.5 Hz) and 8 are pop song cases. The tests that involved a metronome cue had the duration of 35 seconds and 60 seconds for those involving a pop song.

In the following sections, the bouncing motion is analyzed based on the clavicle accelerations measured in the experiment. Figure 5 shows the time history of a clavicle acceleration record of a participant bouncing at 1.8 Hz. For each record, the first and last three seconds (marked by the dashed lines in Figure 5) are discarded to exclude the influence of the irrelevant initialization and the ceasing part of the bouncing motion.

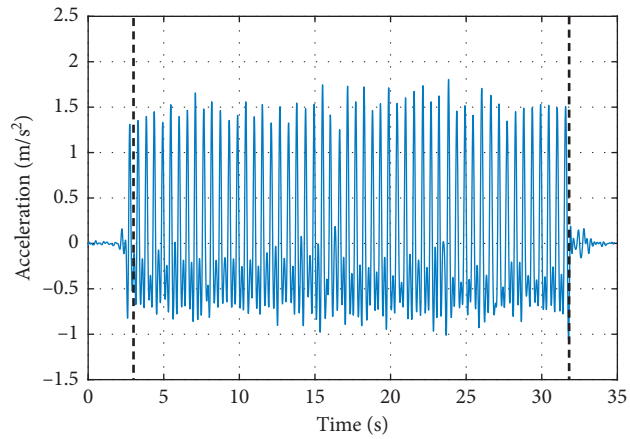

Figure 5: Clavicle acceleration of Participant No. 18 (solid) with cutting lines (dashed) bouncing at 1.8 Hz.

3. Data Processing and Analysis

This section introduces the following quantities to analyze the individual and the collective crowd-bouncing motion: the mean value (Section 3.1) and equivalent bandwidth of the achieved bouncing frequency (Section 3.2), the correlation and the coordination factor (Section 3.3), and the spatial coherence (Section 3.4). Unless otherwise specified, records from the $1\,\text{m} \times 1\,\text{m}$ spacing configuration are adopted for the following illustrative analysis.

3.1. Probability Distribution of Achieved Bouncing Frequency. The achieved bouncing frequency f_s (Hz) is defined as the frequency corresponding to the peak value of the fundamental harmonic of the individual power spectral density (PSD) of the clavicle acceleration (Figure 6). The PSDs are calculated by applying the pwelch function in MATLAB [29]. In this way, the achieved bouncing frequency is determined for each participant in each test. It is then normalized to the metronome frequency f_m (Hz). For the test case of 1.8 Hz, Figure 7 shows the normalized achieved bouncing frequencies of all participants, where each was assigned according to their standing position in a matrix form. Note from Figure 7 that some participants standing at the edge of the crowd were unable to keep up with the metronome beat so that their normalized achieved bouncing frequency deviates far from 1. Records of these participants are denoted as outliers, which were identified by means of a modified score M_i suggested by Iglewicz and Hoaglin [30]:

$$M_i = \frac{0.6745\,(x_i - \tilde{x})}{\text{MAD}}, \tag{2}$$

with MAD denoting the median absolute deviation and $\tilde{x}$ denoting the median. The median absolute deviation is a measure of statistical dispersion and is a robust statistic, being more resilient to outliers in a data set than the standard deviation. Following the recommendations of [30], data entries corresponding to an absolute value of the modified score M_i which is greater than 3.5 are labelled as outliers and, thus, excluded from the data set. The analysis shows that the number of outliers is about 1–7 participants in each test case; that is, 2%–14% persons in the crowd are nonsynchronous participants and are excluded from further statistical analysis.

Figure 8 shows the probability density function (PDF) of the normalized achieved bouncing frequency identified for all participants for the test case with a metronome frequency of 2.1 Hz. This figure shows that the PDF of the achieved bouncing frequency can be well approximated by a normal distribution. A similar observation is made for the other test cases.

The calculated mean values and standard deviations of the achieved frequency for all metronome-guided cases are shown in Figure 9. A slightly decreasing trend of achieved bouncing frequency can be observed. The results indicate

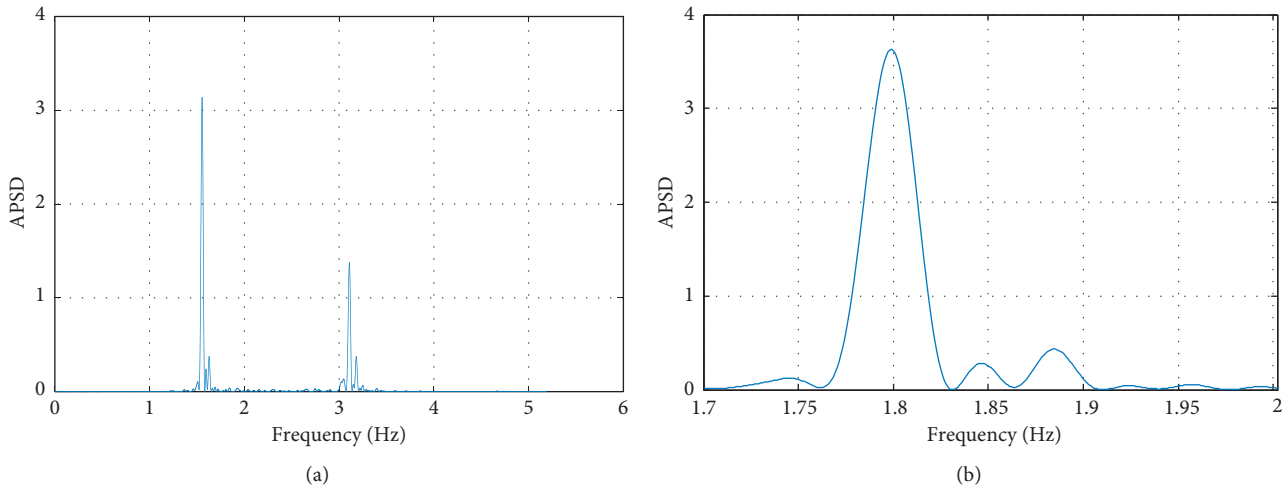

Figure 6: Power spectral density (PSD) of the clavicle acceleration of Participant No. 18 bouncing at 1.8 Hz. The corresponding time series is visualized in Figure 5. (a) Full view; (b) Zoom view.

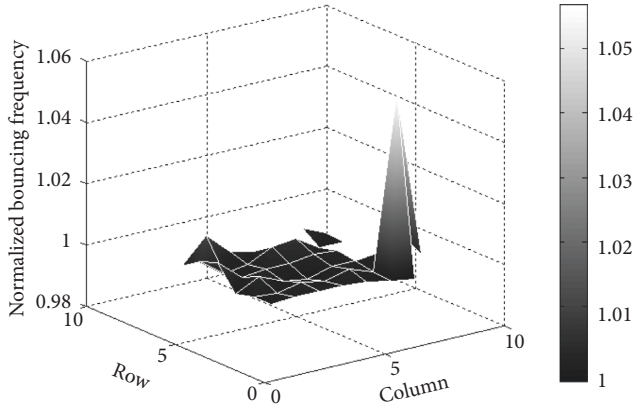

Figure 7: Normalized achieved bouncing frequencies for participants with 1 m × 1 m spacing at 1.8 Hz in one test.

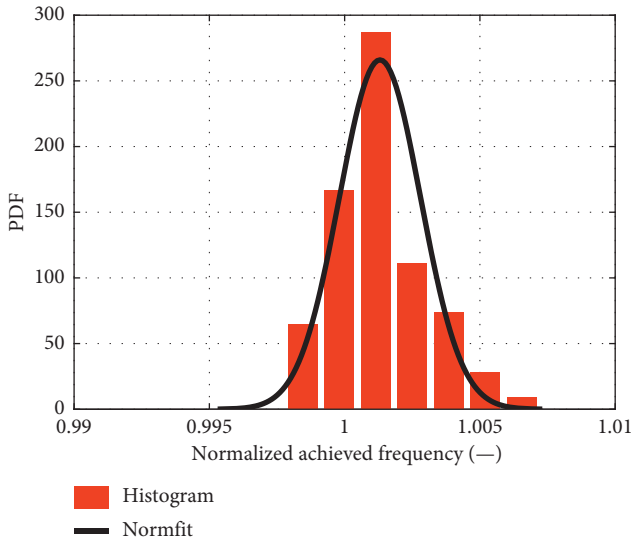

Figure 8: PDF of normalized achieved bouncing frequencies for all participants for the reference configuration at 1.8 Hz.

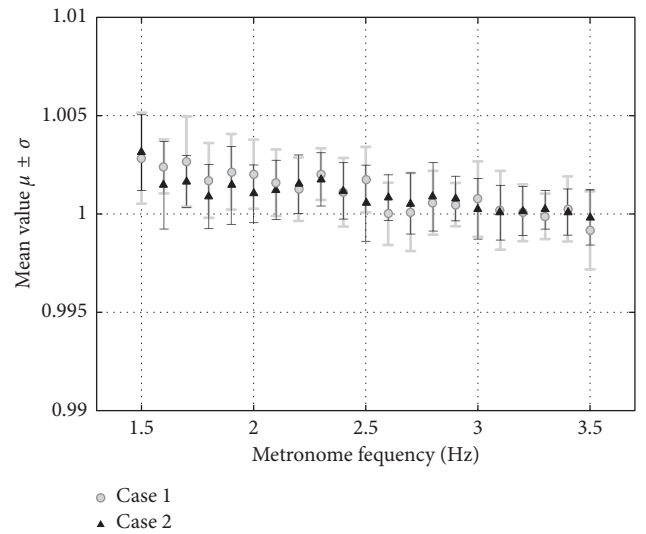

Figure 9: Distribution summary of normalized achieved frequencies in two tests for the reference configuration.

that, at low and medium frequencies ($f_m \leq 2.5$ Hz), participants bounce faster than the metronome beat, indicating that the rhythm is uncomfortably slow. As the metronome frequency increases, it becomes easier for participants to follow the indicated rhythm. At intermediate frequencies ($2.6\,\text{Hz} \leq f_m \leq 3.4\,\text{Hz}$), the mean values of the normalized bouncing frequency are close to unity, which suggests that the metronome tempo is easily followed, thereby allowing better synchronization among the crowd. At the highest frequency ($f_m = 3.5$ Hz), it is difficult for the participants to keep up with the tempo, resulting in a lower mean value than unity.

It is illustrated in Figure 6(a) that the bouncing load energy is mainly distributed around the first main harmonics (i.e., frequencies at 1, 2, and 3 times the f_p). Unlike the walking load where the subharmonics can be clearly observed [31], they are barely observable for the bouncing

load. Therefore, the subharmonics of the bouncing load are not considered here.

3.2. Equivalent Bandwidths. Human-induced loading is known to be a narrow-band random process [32, 33], which also applies to the bouncing load that is at focus in this study. The narrow-band nature of bouncing loads can be observed from the distribution of energy around the main harmonics of the bouncing load's power spectral density (PSD) or, in this case, the clavicle acceleration, as illustrated in Figure 6. In this section, the narrow-band nature is characterized by the equivalent bandwidth of the fundamental harmonic of the PSD. According to the equivalent noise bandwidth theory [34], the equivalent bandwidth B_{eq} (Hz) herein is defined as

$$B_{\mathrm{eq}} = \frac{1}{S_{xx}(f_{\mathrm{s}})} \int_{0.5f_{\mathrm{s}}}^{1.5f_{\mathrm{s}}} S_{xx}(f)df, \tag{3}$$

where $S_{xx}(f_{\mathrm{s}})$ is the peak value of the PSD at the achieved bouncing frequency and f (Hz) is the integration variable. Equation (3) is used to calculate the equivalent bandwidth for each participant in the crowd. Figure 10 illustrates the probability density function of the equivalent bandwidth for all participants with the test metronome frequency of 1.8 Hz. This figure shows that the distribution of the equivalent bandwidth of all participants can be well approximated by a normal distribution. Similarly, a good fit is found for the equivalent bandwidth of the PSD for other test cases. In the following, the distribution results are represented through the mean value and corresponding standard deviation of the equivalent bandwidth. Figure 11 presents the results for the 1 m × 1 m configuration. It illustrates the low, yet non-negligible, distribution of the bouncing energy of the PSD around the fundamental harmonic frequency. The largest values for the equivalent bandwidth are found at low frequencies (1.5 Hz), thereby confirming the observation in Section 3.2 that 1.5 Hz is an uncomfortably low rhythm for bouncing. The lowest values for the equivalent bandwidth are found at around 3.4 Hz. This low intraperson variability in bouncing frequency illustrates that, for frequencies from 3.0 to 3.4, it is easier for the participants to follow the metronome beating. The equivalent bandwidth slightly increases again when the metronome frequency becomes higher than 3.4 Hz.

A quadratic function, equation (4), is fitted to the mean value of the equivalent bandwidth for the 1 m × 1 m configuration. For a certain bouncing frequency f_{m} in the range of 1.5 to 3.5 Hz, the distribution range of load energy can be estimated by calculating the equivalent bandwidth:

$$B_{\mathrm{eq,mean}} = af_m^2 + bf_{\mathrm{m}} + c, \quad 1.5\,\mathrm{Hz} \le f_m \le 3.5\,\mathrm{Hz}, \tag{4}$$

where $B_{\mathrm{eq,mean}}$ is the fitted value of the equivalent bandwidth, f_{m} is the metronome frequency, $a = 2.844 \times 10^{-3}$, $b = -1.903 \times 10^{-2}$, and $c = 4.276 \times 10^{-2}$.

3.3. Variation of Synchronization with Frequency and Crowd Size. In this section, the overall synchronization of the crowd is analyzed. The objective is to analyze the level of contribution of each individual to the overall motion of

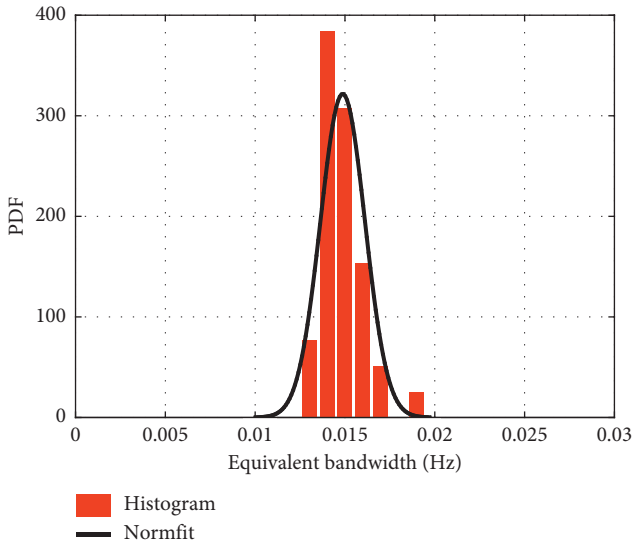

Figure 10: Equivalent bandwidth distribution for all participants at 1.8 Hz for the reference configuration.

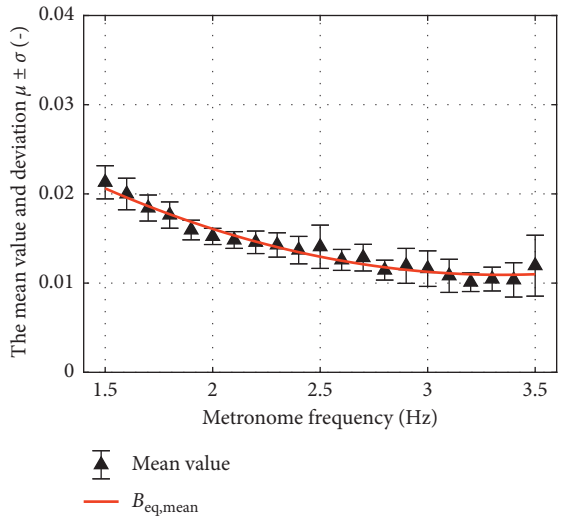

Figure 11: Summary of mean values and standard deviations of equivalent bandwidth for the reference configuration.

the crowd. The synchronous acceleration time history is defined as the average of the overall crowd motion:

$$\ddot{u}_{\mathrm{crowd}}(t) = \frac{1}{N} \sum_{i=1}^{N} \ddot{u}_{\mathrm{cla},i}(t), \tag{5}$$

where $\ddot{u}_{\mathrm{cla},i}(t)$ is the individual clavicle acceleration and N is the number of participants. The motion of the individuals and synchronous crowd motion are shown in Figure 12 for the reference load case with the metronome frequency of 1.8 Hz. Figure 12 shows that the individual motion is similar to the overall crowd motion. However, the individual motion appears not always to be in phase with the overall crowd motion. As a result, the amplitude of the synchronous acceleration is lower than the one reached by most individuals. If all individuals are perfectly synchronized, the amplitude of the overall crowd motion

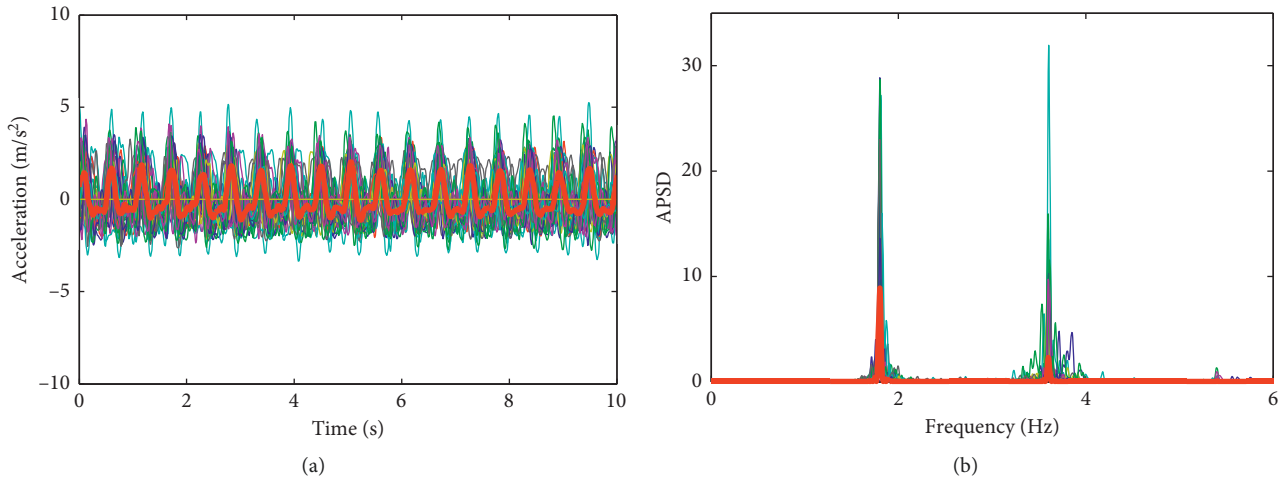

Figure 12: Time histories of the synchronous acceleration (thick red line) and the individual accelerations for the reference load case at 1.8 Hz. (a) Time histories; (b) autopower spectral density.

would be equal to the average amplitude reached by the individuals.

The overall synchronization of the crowd is defined as the coordination factor ρ [14]:

$$\rho = \frac{A_{\text{crowd}}(f_s)}{(1/N)\sum_{i=1}^{N} A_i(f_s)}, \tag{6}$$

where $A_{\text{crowd}}(f_s)$ and $A_i(f_s)$ are the peak Fourier amplitudes which correspond to the dominant frequency of the overall crowd motion acceleration and individual clavicle acceleration, respectively. The coordination factor ρ ranges from 0 to 1. Values of ρ close to 1 indicate a good synchronization of the crowd. On the contrary, ρ values close to zero are a sign of poor synchronization.

Figure 13 shows the variation of coordination factors with bouncing frequencies for the reference configuration. The coordination factor decreases with increasing frequency. The maximum of coordination factor is achieved at 1.7 and 1.9 Hz. At frequencies smaller than 2.6 Hz, the coordination factors are almost above 0.8. When the frequency increases above 2.6 Hz, the synchronization clearly decreases. This indicates that the crowd has the capacity of adjusting the synchronization at moderately high frequencies, while at high frequencies, they have to focus more on following the metronome beat instead of adjusting to the behavior of others.

Then, the Monte Carlo sampling method [35] is used to calculate the synchronization degree of different numbers of persons. The number of persons N_p is changed from 1 to the effective number N_e which is the rest of 48 after excluding the outliers. During each simulation, N_p records of acceleration are randomly selected from N_e records of acceleration and used to calculate the coordination factor by equation (6). For every number "N_p," the simulation is repeated 1000 times, and it turns out that the probability of each record which is selected follows the uniform distribution. Figure 14 shows variation of the mean values of coordination factors obtained from the simulation with different numbers of persons at the frequency of 1.8 Hz. For $N_p = 1$, there is no doubt that the coordination factor equals

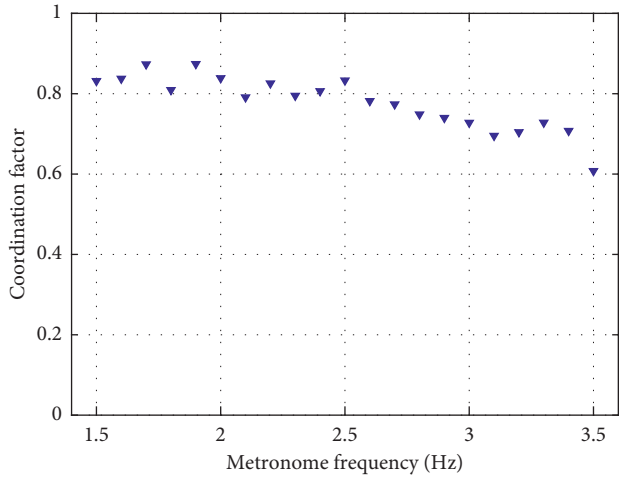

Figure 13: Summary of coordination factors identified from the peak value of the Fourier spectrum of the overall crowd and individual motion for the reference configuration.

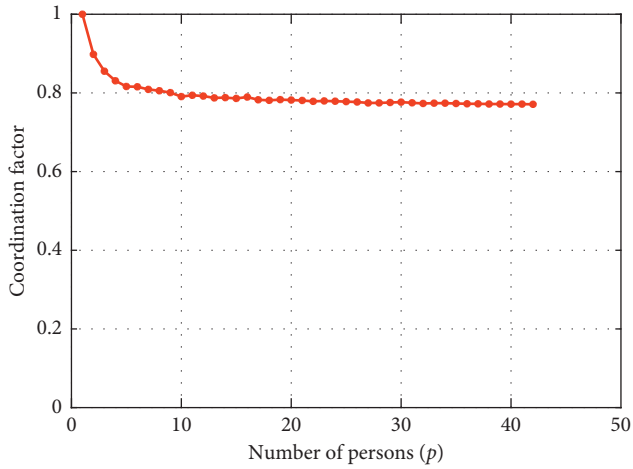

Figure 14: Mean value of coordination factors with different numbers of persons for the reference configuration at 1.8 Hz.

one. Then, the coordination factor obviously decreases with the increasing number of persons. However, the downward trend becomes gradual when the number of persons reaches 10. When the number is larger than 20, the factor becomes steady at around 0.80. For other frequencies, there are similar tendencies of the coordination factor changing with the number of persons. As the factors with maximum persons are different, which can be seen from Figure 13, their descending slopes are different.

3.4. Correlation and Time Lag. The overall synchronization of the whole crowd and between each two participants can also be described by *time lag*, which can be obtained by calculating the cross-correlation of two signals in the time domain. For two signals x_i(t) and x_j(t), their cross-correlation function $R_{ij}(\tau)$ can be calculated by equation (7). The normalized $R_{ij}(\tau)$ varies in the range [0, 1], and the higher the value the more similar the two signals:

$$R_{ij}(\tau) = E\left[x_i(t)x_j(t+\tau)\right]. \quad (7)$$

The value of τ corresponding to the maximum value of $R_{ij}(\tau)$ is chosen as the time lag between x_i(t) and x_j(t), which varies in the range $[-1/(2f_s), 1/(2f_s)]$. First, the correlation between the time histories of an individual and the overall crowd motion (equation (5)) is analyzed. When the time lag is close to zero, it means that this individual is making a great contribution to the overall crowd motion and is therefore considered to be well synchronized. If the absolute value of the time lag increases, then the level of synchronization for that participant decreases and so does his/her impact on the overall crowd motion. For the 1.8 Hz test case, Figures 15 and 16 show the probability density function and the standard deviation of the time lags being calculated for the reference configuration. The results of all test cases show that the time lag follows a normal distribution. Its mean value is almost equal to zero as it comes from all participants and their mean time history, and its standard deviation is around 0.05.

Second, the cross-correlation between every two participants is calculated to observe the difference of acceleration among participants. Figure 17 shows the probability density function of the calculated time lags between each two accelerations at a metronome frequency of 1.8 Hz for the reference configuration. It follows a normal distribution. The time lags between each two accelerations with other metronome frequencies also follow the normal distribution.

3.5. Coherence. Inspired by the theory of turbulent wind on linear structures [36], Brownjohn et al. [10] suggested the following mathematical model to calculate the bridge response under a crowd of pedestrians via the coherence function:

$$S_z(f) = \psi_z^2 |H(f)|^2 S_{P,1}(f) \int_0^L \int_0^L \psi_{z1}\psi_{z2}\mathrm{coh}(f, z_1, z_2)dz_1dz_2, \quad (8)$$

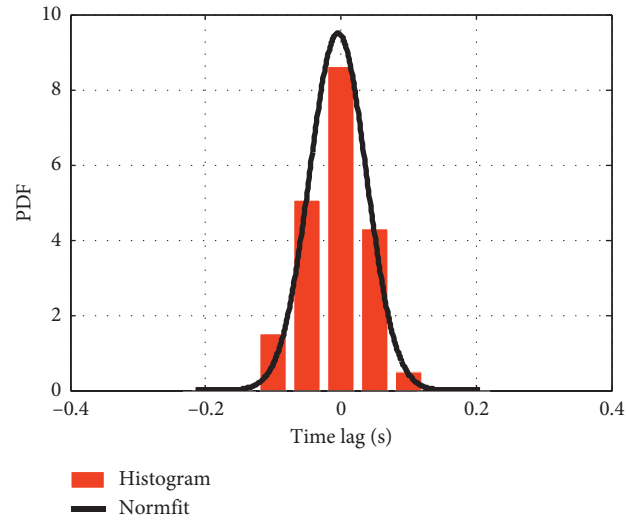

Figure 15: PDF of the time lags identified for the reference configuration at 1.8 Hz.

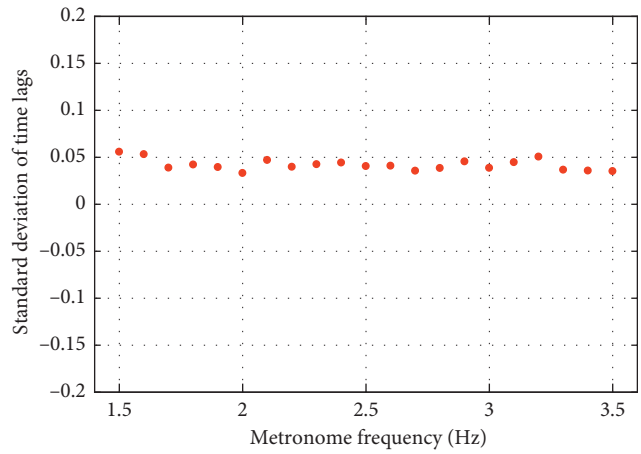

Figure 16: Standard deviation of the time lags of all participants identified for the reference configuration.

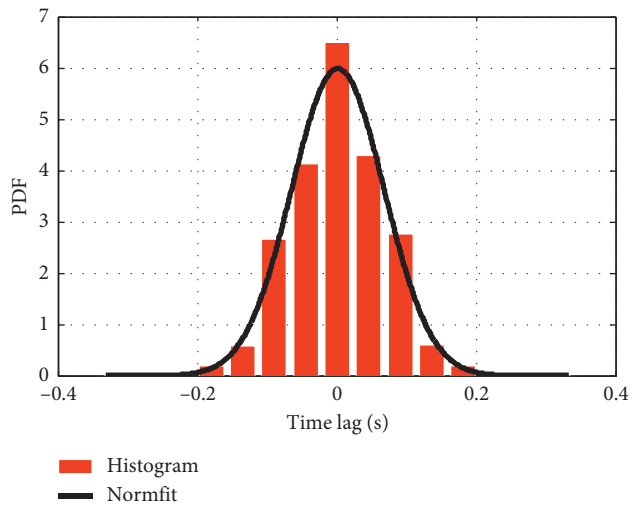

Figure 17: PDF of the time lags between each two participants at 1.8 Hz for the reference configuration.

where $S_z(f)$ is the autopower spectral density (APSD) of the structure response in a single degree of freedom (SDOF) specified by the coordinate z, ψ_z is the mode shape ordinate in the same SDOF, $H(f)$ is the frequency response function (FRF) for the acceleration response, $S_{P,1}(f)$ is the ASD of the pedestrian load per unit length, ψ_{z1} and ψ_{z2} are the mode shape ordinates related to the location of each pair of pedestrians on the bridge described by coordinates z_1 and z_2, and $\mathrm{coh}(f, z_1, z_2)$ is the coherence coefficient, which has a value between zero and one.

The coherence coefficient $|\mathrm{coh}(f_s, d)|$ describes the spatial correlation in a standard random field by equation (9), in which $P_{xy}(f_s)$ is the cross power density spectrum between two signals with the distance d; $P_{xx}(f_s)$ and $P_{yy}(f_s)$ are the autopower density spectra:

$$\left|\mathrm{coh}(f_s, d)\right| = \sqrt{\frac{\left|P_{xy}(f_s)\right|^2}{\left|P_{xx}(f_s)\right|\left|P_{yy}(f_s)\right|}}. \tag{9}$$

In a crowd, the interaction between people, which affects their behavior, can be considered as the influence of persons standing on the left or right side (termed as lateral interaction) and the influence of persons standing in front of them (frontal interaction). Due to the limited visibility, it is expected that the influence of lateral interaction on crowd synchronization is low. When people attend a music concert or a sport match, most attention is drawn to the performance or players in front of them, which means less attention is paid to the people beside them. However, when the density of the crowd is very high, the influence of the lateral interaction may increase when an additional physical stimulus is introduced. The direct and strong impact of visual stimuli is expected from frontal interaction. In this study, the coherence coefficient is analyzed in both directions.

The configurations considered in the experimental study are composed of six rows and eight columns on the first and second days and six rows and seven columns on the third day. In a row, the distances between two participants considered in the experiments are 1, 2, 3, 4, 5, 6, or 7 meters, while in a column, the distances are 1, 2, 3, 4, or 5 meters. Therefore, there are 42 coherence coefficients at the smallest distance of 1 m and 36 coherence coefficients at a distance of 2 m until the number of coherence coefficients is down to 6 at a distance of 7 m. The coherence coefficient is calculated via the magnitude-squared coherence estimated by MATLAB [29]. The coherence coefficients range from 0 to 1, and most of them are close to 1. To find a well-fitted distribution, the coherence coefficients x_{coh} are substituted by their negative natural logarithm.

In the following, lognormal and Weibull distributions are fitted to the coherence coefficient for different distances. Generally, the lognormal distribution provides a better fit than the Weibull distribution. The lognormal distribution is described as

$$f(x_{\mathrm{coh}}) = \frac{1}{x_{\mathrm{coh}}\sigma_{\mathrm{L}}\sqrt{2\pi}} e^{\left(-\left(\ln x_{\mathrm{coh}} - \mu_{\mathrm{L}}\right)/2\sigma_{\mathrm{L}}^2\right)}, \tag{10}$$

in which $\mathrm{coh} \in (0, 1)$ and $x_{\mathrm{coh}} > 0$.

3.5.1. Lateral Coherence. Figure 18 presents all coherence coefficients and their mean values at lateral distances of 1 m and 2 m. The results show that all mean values of the coherence coefficient are above 0.9 and the mean values at the same frequency for two lateral distances are close. Figures 19(a) and 19(b) show the Weibull and lognormal distributions fitted to the coherence of every two participants with an interperson distance of 1 m and 2 m, respectively. For distances larger than 4 m, no good fit can be obtained due to low coherence as well as lack of data samples. The shape parameters of well-fitted lognormal distributions for distances of 1 m to 4 m are listed in Table 4.

Figure 20 presents variation of the lognormal distribution parameters (mean ± standard deviation) with bouncing frequencies for four lateral distances (1~4 m). Although the results are different for every lateral distance, a similar variation range and tendency is observed.

3.5.2. Frontal Coherence. In Figures 21(a) and 21(b), the frontal coherence coefficients are shown for a longitudinal spacing of 1 m and 2 m. This figure illustrates that the dispersion of coherence coefficients with a metronome frequency between 1.7 Hz and 2.7 Hz is smaller than others. Figure 21 also shows that the mean values with two frontal distances are quite similar, and they are all above 0.9.

Identical to the analysis of the lateral coherence, Figures 22(a) and 22(b) show that a lognormal distribution can be used to describe the frontal coherence between participants. The shape parameters of lognormal distribution are listed in Table 5.

Figure 23 presents variation of the lognormal distribution parameters with bouncing frequencies for three frontal distances. These results show that there is no obvious relation between the parameters and the longitudinal distances, but again a similar tendency is observed when the parameter μ_{L} decreases for frequencies lower than 2 Hz, achieves the lowest point at 2 Hz, and then increases along with the metronome frequency. Note that similar parameters σ_{L} are found for all cases with different distances.

3.5.3. Coherence between Each Two Participants. The above results indicate that distance has limited influence on the coherence coefficient. Therefore, the coherence coefficients between a single participant and each of the participants in the crowd are calculated. Table 6 lists a single example: the results of the participant standing in row six and line two. As expected, the coherence coefficient with himself equals 1.0. All coherence coefficients with other participants are close to or above 0.9. It is observed that this coefficient does not increase or decrease with the distance between two individuals. These results are confirmed in Figure 24 that shows the distribution of all coherence coefficients in terms of the metronome frequency, excluding the duplicate items. If the autopower spectrum density of the reference person is known, then the coherence coefficients $\mathrm{coh}(f, z_1, z_2)$ between that person and any others can be found from

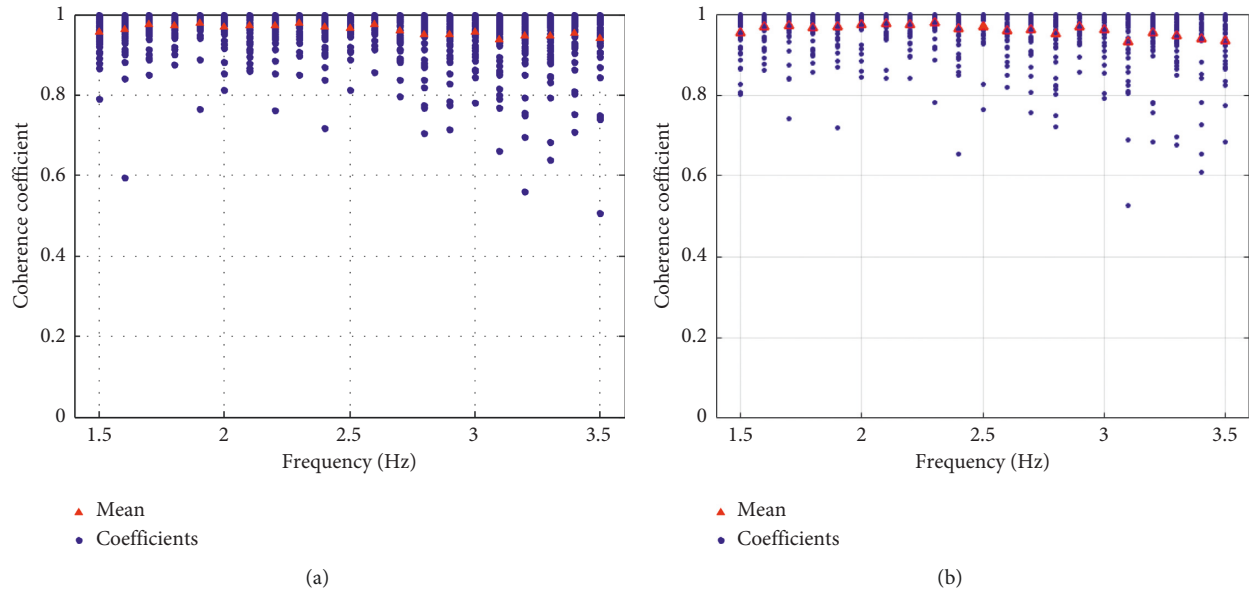

Figure 18: Coherence coefficients of all cases along with frequency at two lateral distances of (a) 1 m and (b) 2 m.

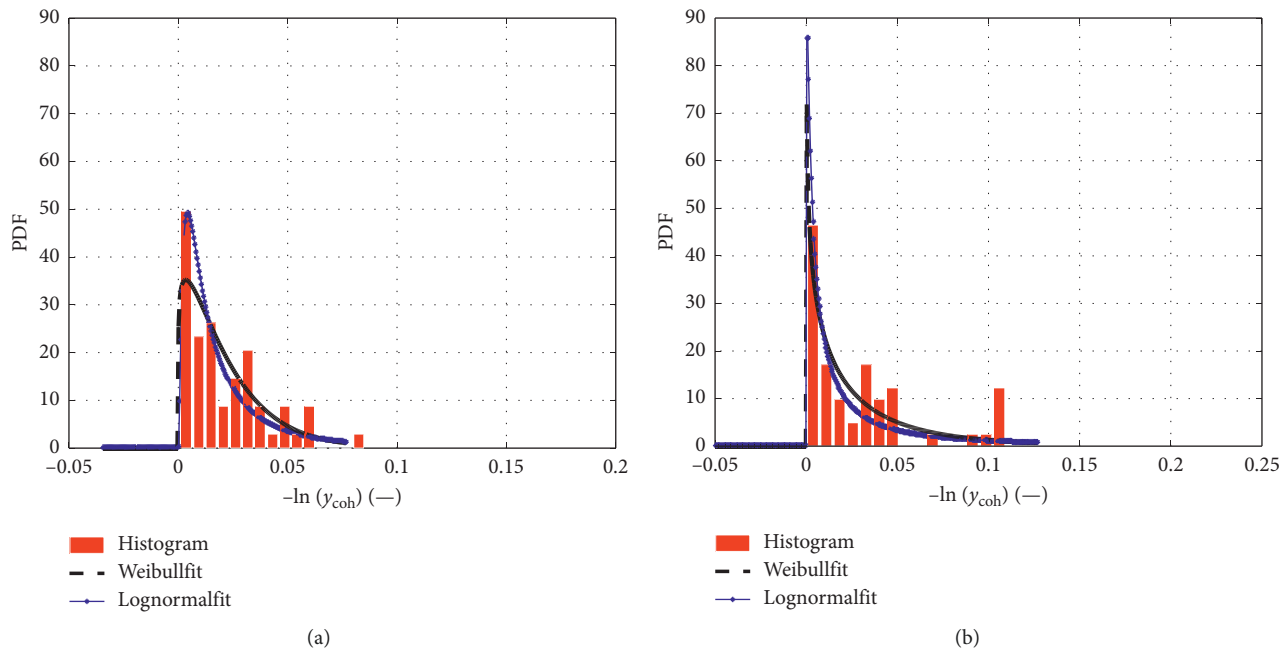

Figure 19: Results for lognormal and Weibull distributions of coherence coefficients at 1.8 Hz with lateral distances of (a) 1 m and (b) 2 m.

Table 6 and then can be used in equation (8). Figure 25 presents the mean values and standard deviations of all coherence coefficients between any two participants along with the metronome frequency. The result shows that the synchronization of crowd in the frequency domain between 1.7 Hz and 2.7 Hz is much better than that in other frequencies due to the higher mean values and smaller standard deviations.

From what has been discussed above, the bouncing crowd can be assumed to be a stationary and homogeneous isotropic field. The stationary process is based on cross-correlation in the time domain (Section 3.4). As the directions and the distances make no obvious difference on coherence coefficients, the homogeneous isotropic refers to the spatial stability which is based on coherence in the frequency domain in this section.

3.6. Summary. Four quantities are introduced to describe the intra- and interperson variability in the fundamental bouncing frequency and the level of synchronization in the crowd.

Table 4: μ and σ in lognormal distribution of coherence coefficients in the lateral direction.

Frequency (Hz)	μ				σ			
	Distance = 1 m	Distance = 2 m	Distance = 3 m	Distance = 4 m	Distance = 1 m	Distance = 2 m	Distance = 3 m	Distance = 4 m
1.5	−3.807	−4.16	−3.762	−3.711	1.272	1.318	1.110	1.210
1.6	−4.205	−4.212	−4.004	−4.204	1.181	1.488	1.430	1.406
1.7	−4.611	−4.873	−4.619	−5.211	1.307	1.391	1.597	1.330
1.8	−4.312	−4.394	−4.707	−4.940	1.070	1.783	1.502	1.016
1.9	−4.665	−4.665	−4.741	−4.768	1.395	1.324	1.483	1.570
2.0	−5.101	−4.911	−4.946	−5.009	1.066	1.183	1.571	1.014
2.1	−4.857	−4.502	−5.015	−4.392	1.320	1.304	1.452	1.401
2.2	−4.643	−4.373	−4.473	−4.983	1.312	1.172	1.471	1.028
2.3	−4.753	−4.852	−5.166	−4.773	1.013	1.551	1.401	1.025
2.4	−5.013	−4.550	−4.407	−4.698	1.499	1.462	1.260	1.376
2.5	−4.107	−5.062	−4.206	−4.107	1.164	1.142	1.332	0.993
2.6	−4.596	−4.084	−4.445	−4.189	1.443	1.332	1.084	1.145
2.7	−4.028	−4.265	−4.425	−3.995	1.530	1.121	1.280	1.290
2.8	−4.023	−4.530	−4.687	−4.818	1.392	1.342	1.185	1.384
2.9	−4.257	−4.236	−3.865	−4.281	1.628	1.638	1.430	1.565
3.0	−4.045	−4.111	−4.385	−4.188	1.261	1.281	1.727	1.728
3.1	−3.866	−3.892	−3.642	−3.654	1.285	1.247	1.583	1.126
3.2	−4.234	−3.897	−3.795	−4.253	1.356	1.069	1.229	1.388
3.3	−3.939	−3.580	−4.554	−4.172	1.171	1.175	1.344	1.360
3.4	−4.192	−4.365	−3.852	−4.111	1.388	1.062	1.073	1.031
3.5	−4.118	−3.423	−3.939	−3.697	1.346	1.284	1.454	1.266

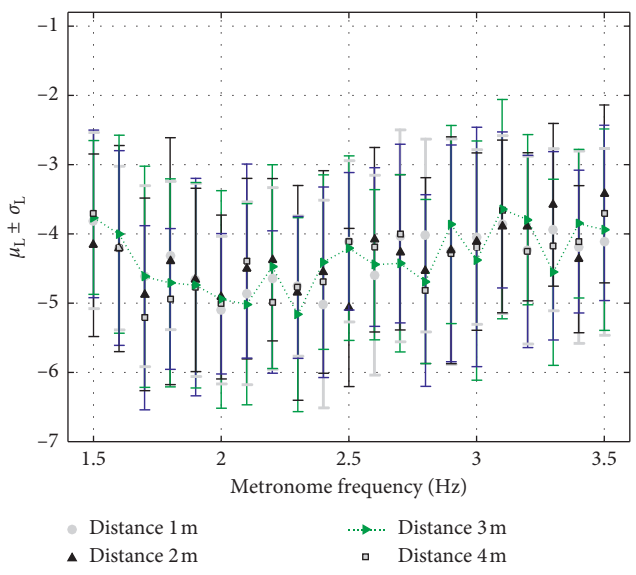

Figure 20: Error bar of lognormal distribution parameters of coherence coefficients in the lateral direction.

3.6.1. Intravariables. The intravariables (achieved bouncing frequency and equivalent bandwidth) indicate the energy distribution of the bouncing individual, and all the other intervariables quantify, from different angles, the relationship among individuals in the bouncing crowd.

For the reference configuration 1 m × 1 m with 21 metronome frequencies, the intraperson variability of the achieved bouncing frequencies and corresponding equivalent bandwidth follow a normal distribution. For the considered range of metronome frequencies (1.5 Hz to 3.5 Hz), the normalized achieved bouncing frequency is characterized by a downward tendency corresponding to the metronome frequency. A quadratic relation is found between the metronome frequency and the equivalent bandwidth of the fundamental bouncing frequency, illustrating that the rhythms between 3.0 Hz and 3.4 Hz are the easiest for participants to follow.

3.6.2. Intervariables. Concerning the cross-correlation, the time lags are found to follow a normal distribution, and their standard deviation varies around 0.05 (s). In turn, the correlation values vary with the metronome frequency like a quadratic function, and its standard deviation varies within a range from 0.05 to 0.15. The coordination factors are observed to decrease with the metronome frequency, indicating that the coordination among crowd is getting worse when the participants bounce faster and faster. For lateral and frontal coherence coefficients and that between any two participants, the lognormal distribution can be used to specify the probability of the negative natural logarithm coherence coefficients. The results of this study also show that the locations of and distance between persons in a bouncing group have little influence on the coherence coefficients, which can be used to simplify the crowd load modelling in the frequency domain.

4. Influence of Various Stimuli on the Behavior of the Bouncing Crowd

In this section, the quantities introduced in the previous section are used to analyze the influence of various

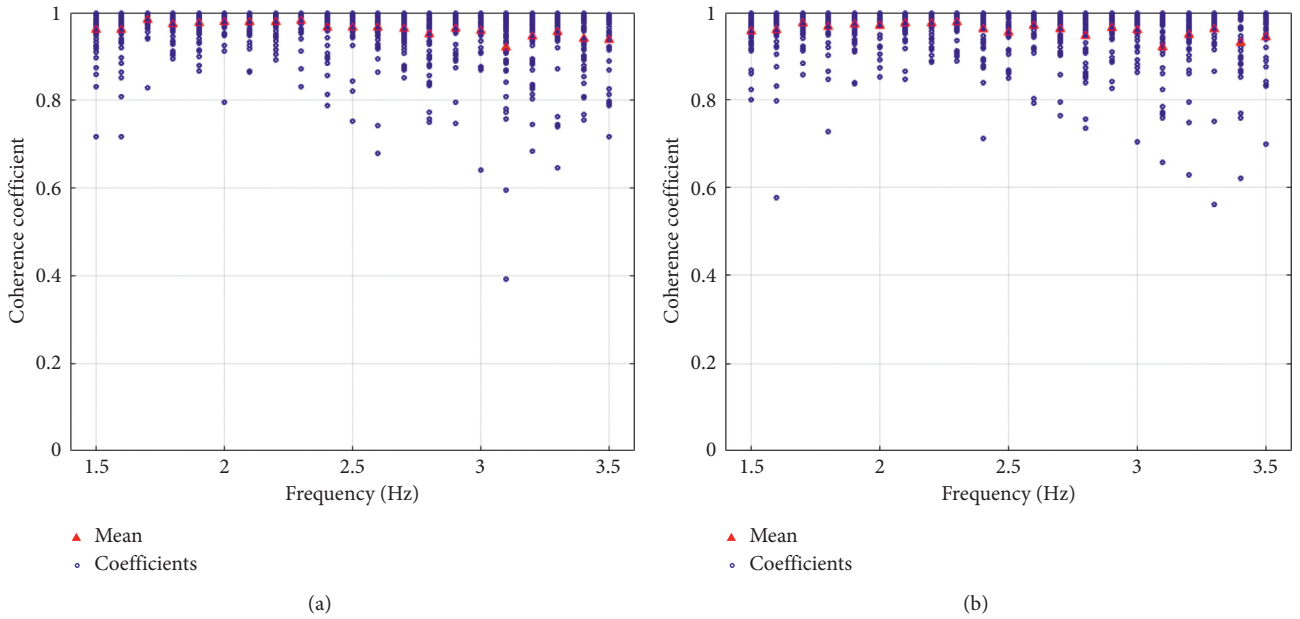

Figure 21: Coherence coefficients of all cases along with metronome frequency at two frontal distances of (a) 1 m and (b) 2 m.

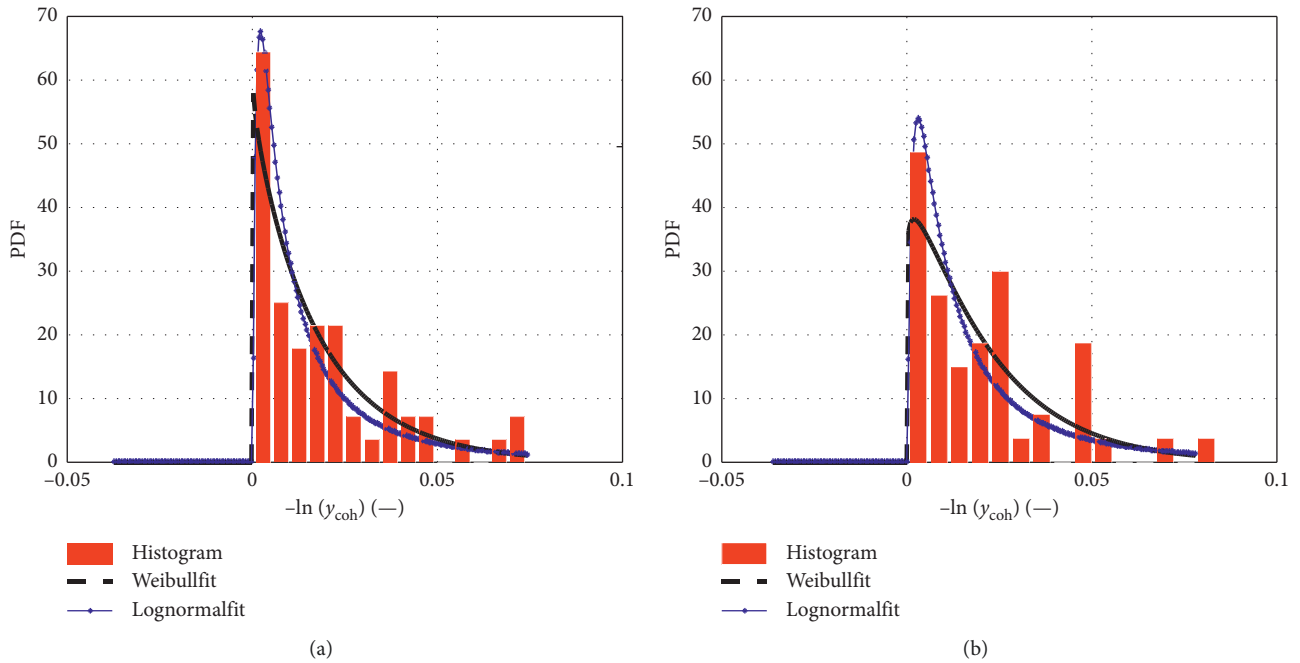

Figure 22: Results for lognormal and Weibull distributions of coherence coefficients at 1.8 Hz with frontal distances of (a) 1 m and (b) 2 m.

parameters: spatial configuration (Section 4.1), visual stimuli (Section 4.2), and auditory stimuli (Section 4.3).

4.1. Influence of the Spatial Configuration. In total, six configurations (thus different crowd densities) were considered in the experimental study (see Table 3). To investigate the influence of the spatial configuration, the considered configurations are divided into two groups. In Table 7, group 01 and group 02 are characterized by the same frontal and lateral distances, respectively: group 01 configurations are 1×1, 1×0.6, and 1×0.8 and group 02 configurations are 1×1, 0.8×1, and 1.2×1. The interval distance between two neighbouring participants is referred to as the single distance. Then, after multiplying the number of segments, there are five single distances in a column and seven single distances in a row. Note that $1\,\text{m} \times 1\,\text{m}$ is the reference configuration.

Table 5: μ and σ in lognormal distribution of coherence coefficients in the longitudinal direction.

Frequency (Hz)	μ			σ		
	Distance = 1 m	Distance = 2 m	Distance = 3 m	Distance = 1 m	Distance = 2 m	Distance = 3 m
1.5	−3.9201	−3.911	−4.204	1.179	1.446	1.466
1.6	−4.043	−4.626	−4.084	1.068	1.830	1.240
1.7	−4.877	−4.441	−4.183	1.421	1.107	1.106
1.8	−4.578	−4.372	−4.267	1.247	1.196	1.411
1.9	−4.916	−4.988	−4.801	1.391	1.051	0.999
2.0	−5.448	−5.315	−5.119	0.970	1.760	1.410
2.1	−4.877	−4.511	−4.480	1.517	1.298	1.162
2.2	−4.561	−5.176	−4.832	1.165	1.626	1.328
2.3	−4.945	−4.918	−4.903	1.549	1.267	1.232
2.4	−4.446	−4.514	−4.634	1.274	1.504	1.526
2.5	−4.230	−3.743	−4.266	1.105	1.532	0.804
2.6	−5.059	−5.057	−4.546	1.525	1.318	1.400
2.7	−4.093	−4.330	−4.564	1.227	1.550	1.999
2.8	−4.233	−3.999	−4.389	1.618	1.625	1.266
2.9	−4.573	−4.438	−4.751	1.128	1.060	1.486
3.0	−3.884	−4.020	−4.004	1.183	1.270	1.653
3.1	−3.298	−3.417	−3.309	1.268	1.485	1.193
3.2	−3.807	−3.850	−3.930	1.173	1.421	1.402
3.3	−4.040	−4.407	−3.641	1.097	1.507	0.882
3.4	−3.686	−3.527	−3.828	1.405	1.556	1.324
3.5	−3.678	−4.165	−3.653	0.954	1.668	0.842

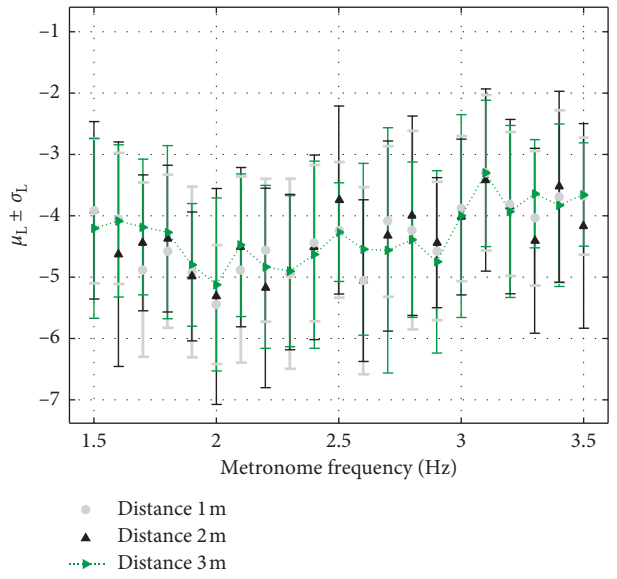

Figure 23: Error bar of lognormal distribution parameters of coherence coefficients in the frontal direction.

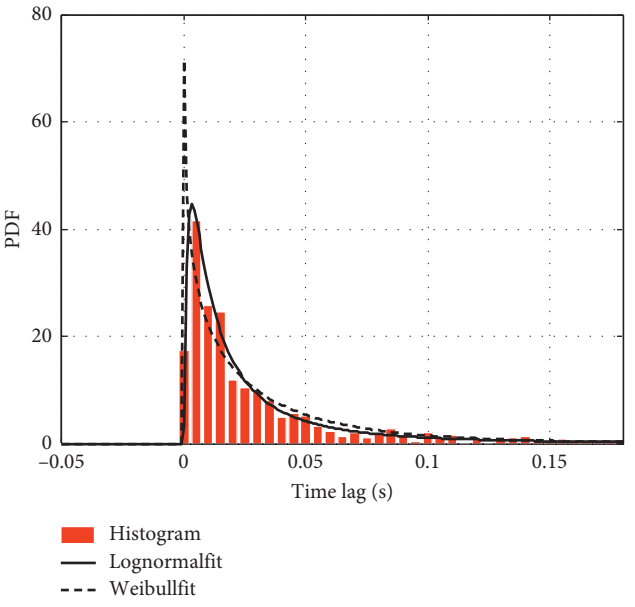

Figure 24: Distribution results of coherence coefficients between each two participants at 1.8 Hz for the reference configuration.

Table 6: Coherence coefficients of a single participant (bold) with others at 1.8 Hz

0.9844	0.9966	0.9901	0.9073	0.9972	0.9956	—	—
0.9858	0.9940	0.8489	0.9869	0.9962	—	—	0.9696
0.9983	0.9940	0.9885	0.9630	0.9995	0.9986	0.9747	0.9930
0.9931	0.9839	0.9976	0.9789	0.9993	0.9975	—	0.9943
0.9014	0.9914	0.9910	0.9981	0.9176	0.9887	0.9928	0.9633
0.9939	**1.0000**	0.9682	0.9971	—	0.9966	—	—

4.1.1. Normalized Achieved Bouncing Frequency and Equivalent Bandwidth. Figures 26 and 27 provide no evidence indicating that lateral or frontal distances have a clear effect on the normalized achieved bouncing frequency and equivalent bandwidth.

In Figures 26(a) and 26(b), a similar downward tendency of the mean values of the normalized achieved bouncing frequency is observed with the metronome frequency. Although there is a mildly decreasing trend of these mean values, the difference between the maximum and minimum is less than 2%. In both groups, the standard deviations of the other two configurations except for the reference one all become smaller along with the metronome frequency. All standard deviations are smaller than 0.3%.

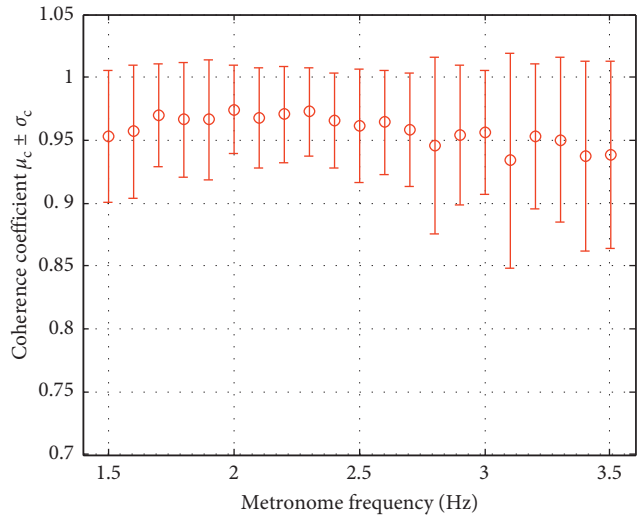

Figure 25: Error bar of coherence coefficients between each two participants for the reference configuration.

Table 7: Configurations of groups according to lateral and frontal distances.

Group	Name	Configuration	Longitudinal distance (column)	Lateral distance (row)
01	P0	1 × 1	1, 2, 3, 4, 5	1, 2, 3, 4, 5, 6, 7
	P1	1 × 0.6		0.6, 1.2, 1.8, 2.4, 3.0, 3.6, 4.2
	P2	1 × 0.8		0.8, 1.6, 2.4, 3.2, 4.0, 4.8, 5.6
02	P0	1 × 1	1, 2, 3, 4, 5	1, 2, 3, 4, 5, 6, 7
	P3	0.8 × 1	0.8, 1.6, 2.4, 3.2, 4.0	
	P4	1.2 × 1	1.2, 2.4, 3.6, 4.8, 6.0	

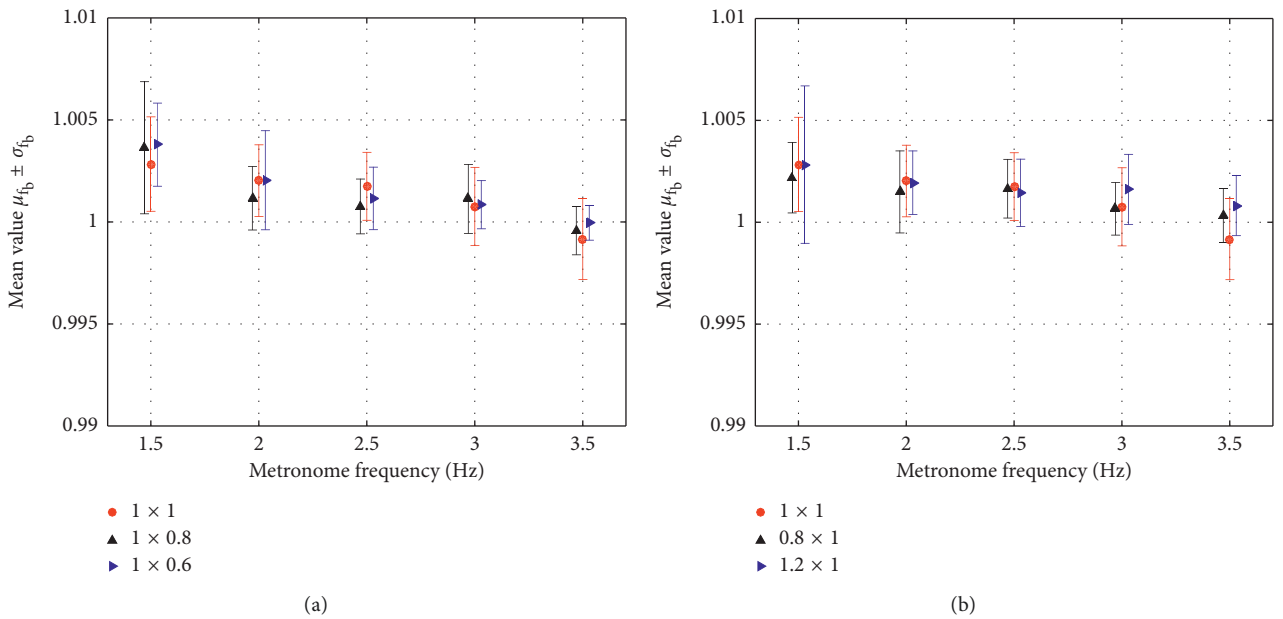

Figure 26: Comparison of normalized achieved bouncing frequency with three configurations in two groups. (a) Group 01 with different lateral distances; (b) group 02 with different frontal distances.

Figure 27 shows the statistical results of the equivalent bandwidth for different spatial configurations. In all cases, the largest equivalent bandwidth is found for the lowest frequency, i.e., 1.5 Hz. As for the reference configuration, the same downward tendency for the equivalent bandwidth with the metronome frequency is found. A minimum bandwidth is reached for 3.0 Hz, after which the mean value of the equivalent bandwidth increases together with the standard deviation.

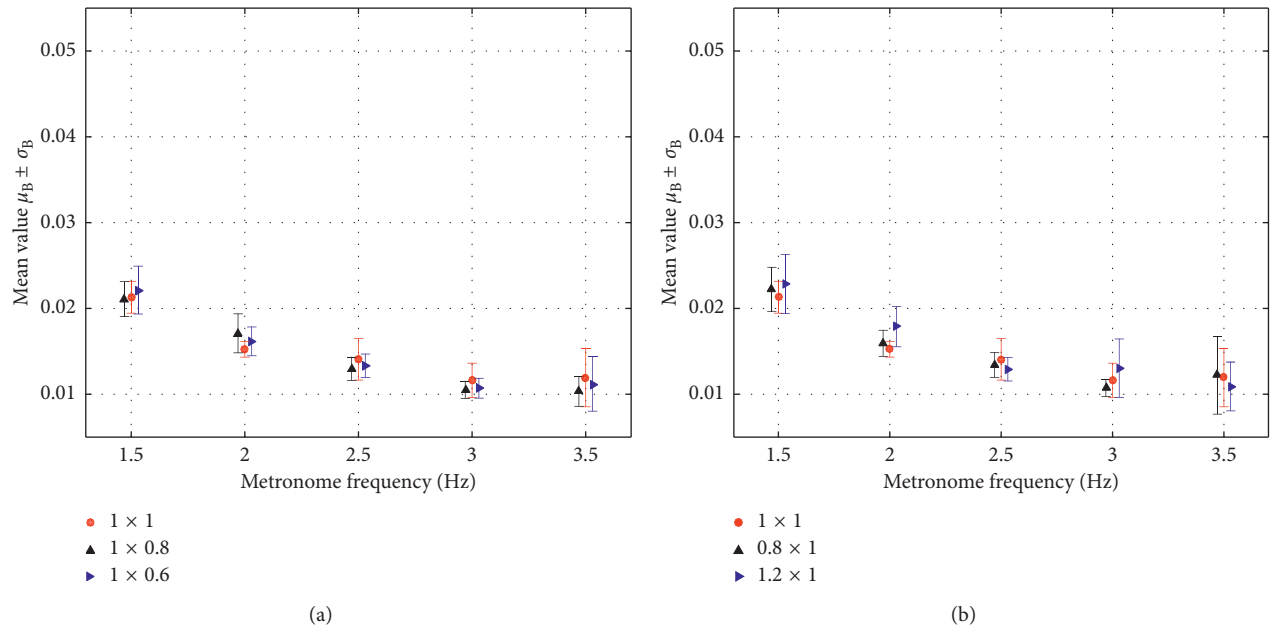

Figure 27: Comparison of equivalent bandwidth with three configurations in two groups. (a) Group 01 with different lateral distances; (b) group 02 with different frontal distances.

4.1.2. Time Lag and Coordination Factor. In Figure 28, comparison of the time lags of three spatial configurations in two groups is presented. There is no clear relation among the results from different spatial configurations. The results from different groups are also compared. In all cases, the largest standard deviations of time lags are observed at a metronome frequency of 1.5 Hz.

Figure 29 shows that similar coordination factors can also be obtained for all the spatial configurations. The highest coordination factors are obtained at 2.0 Hz for all configurations in group 02 and the reference configuration in group 01. For the other two configurations in group 01, the metronome frequency is set at 2.5 Hz, while the lowest coordination factors are obtained for all configurations in both groups at 3.5 Hz.

4.1.3. Coherence Coefficient. For distances larger than 3 m, the coherence coefficient is too low to be discussed. The parameters (μ_L, σ_L) of the lognormal PDFs of the coherence coefficients for different configurations of group 01 and group 02 are shown in Figures 30(a) and 30(b). Figure 31 presents similar results for two groups with double distances. Again, no clear impact of the spatial configuration is observed.

Apart from the coordination factor which (slightly) increases with decreasing frontal distance, no relevant impact on the inter- and intraperson variability was observed, neither in the bouncing motion nor in the global crowd behavior for the considered spatial configurations.

4.2. Influence of Visual Stimuli. To investigate the impact of visual stimuli, the tests in the reference configuration are repeated with and without an eyepatch. These tests are performed for 21 metronome frequencies and 10 song-enhanced test cases (see Table 3).

4.2.1. Normalized Achieved Bouncing Frequency and Equivalent Bandwidth. Figure 32 shows the PSDs of two participants bouncing with and without an eyepatch for 1 m × 1 m at 1.8 Hz. Figure 32(a) shows that when an eyepatch is used, the lack of visual stimuli results in a significant increase of the intraperson variability; thus, the bouncing energy disperses around the harmonics, and the peak value of the energy is much lower. However, the impact is not equally significant for every participant. More than 70% of participants' bouncing energy follows a distribution pattern, as shown in Figure 32(b). Figures 33 and 34 illustrate the comparison of the normalized achieved bouncing frequency and the equivalent bandwidth, with and without visual stimuli. In both cases, the mean value of the normalized bouncing frequency is similar, although its value appears to be closer to unity when no eyepatch is worn. From Figure 34, a (small) increase is observed in the standard deviation of the equivalent bandwidth when the eyepatch is used. This indicates that, with an eyepatch, the bouncing energy is more dispersive because the eyepatch introduces some uncertainty in the human behavior, causing some to feel less in control.

4.2.2. Time Lag and Coordination Factor. Figure 35 shows the comparison of the time lags and correlation values for the cases with and without eyepatches. Figures 35(a) and 35(b) indicate the same point where the correlation value with an eyepatch is lower than that for the reference configuration and the time lags are higher. In Figure 36, the tendency of coordination factors indicates the same

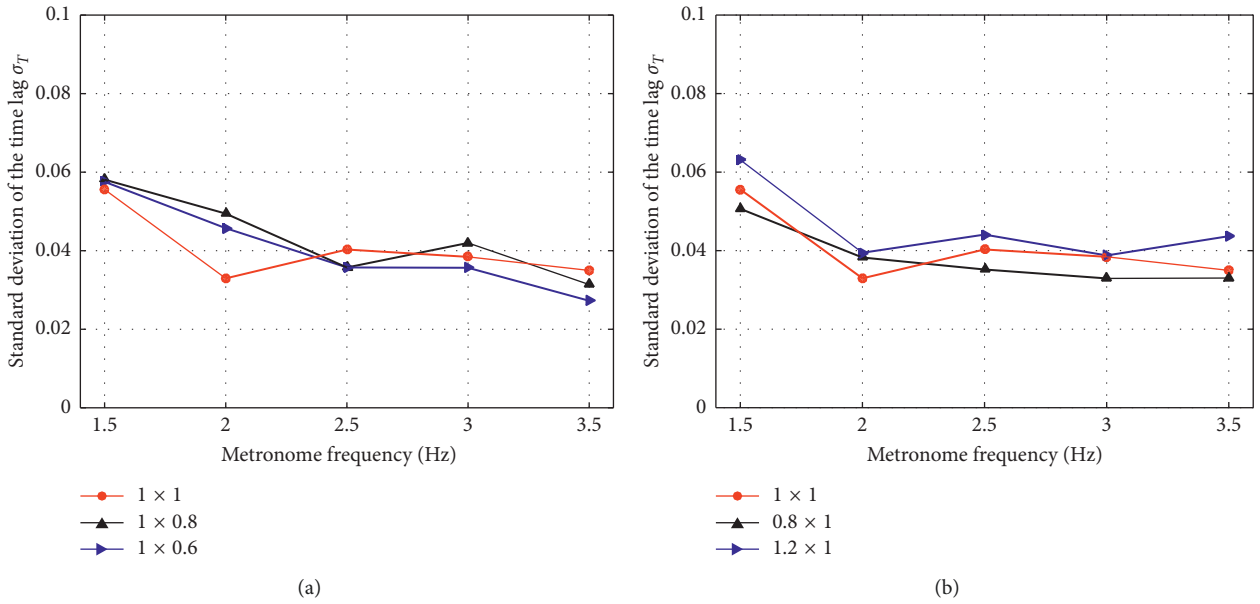

Figure 28: Comparison of the time lags with three configurations in two groups. (a) Time lags in group 01; (b) time lags in group 02.

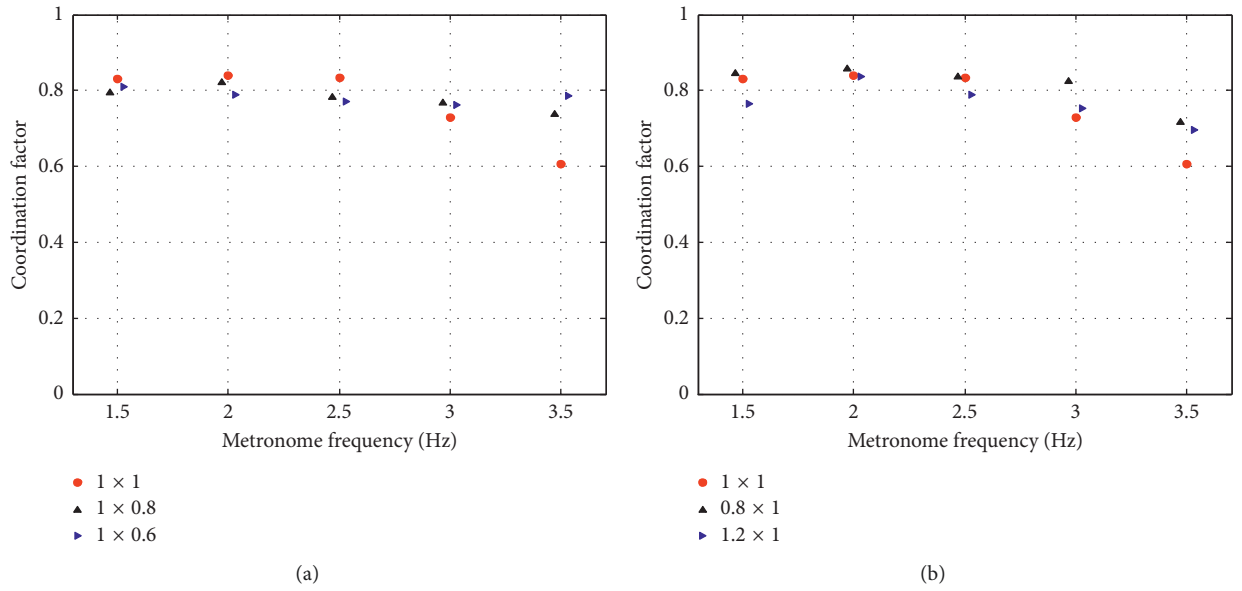

Figure 29: Comparison of coordination factors with three configurations in two groups. (a) Coordination factors in group 01; (b) coordination factors in group 02.

conclusion. With an eyepatch, the coordination factor is lower. Their concentration may be more significant when getting a visual effect from others to improve the level of synchronization.

4.2.3. Coherence Coefficient. Figure 37 shows the comparison of the mean values of the coherence coefficients in lateral and frontal directions for visual stimuli, with and without an eyepatch. There is no obvious influence of the visual stimuli on both lateral coherence and frontal coherence.

Visual stimuli have a positive impact on individual bouncing statistics, especially for those who might feel uncertain about their bouncing behavior. On the contrary, the results of correlation and coordination indicate that the level of synchronization is higher when participants wear the eyepatch.

From the more dispersive energy distribution of individual PSD and lower coordination factor with an eyepatch, it is indicated that each individual's behavior is affected by his own sense of safety and surrounding pedestrians via visual connection. However, it is impossible to separate these two irregular effects with these

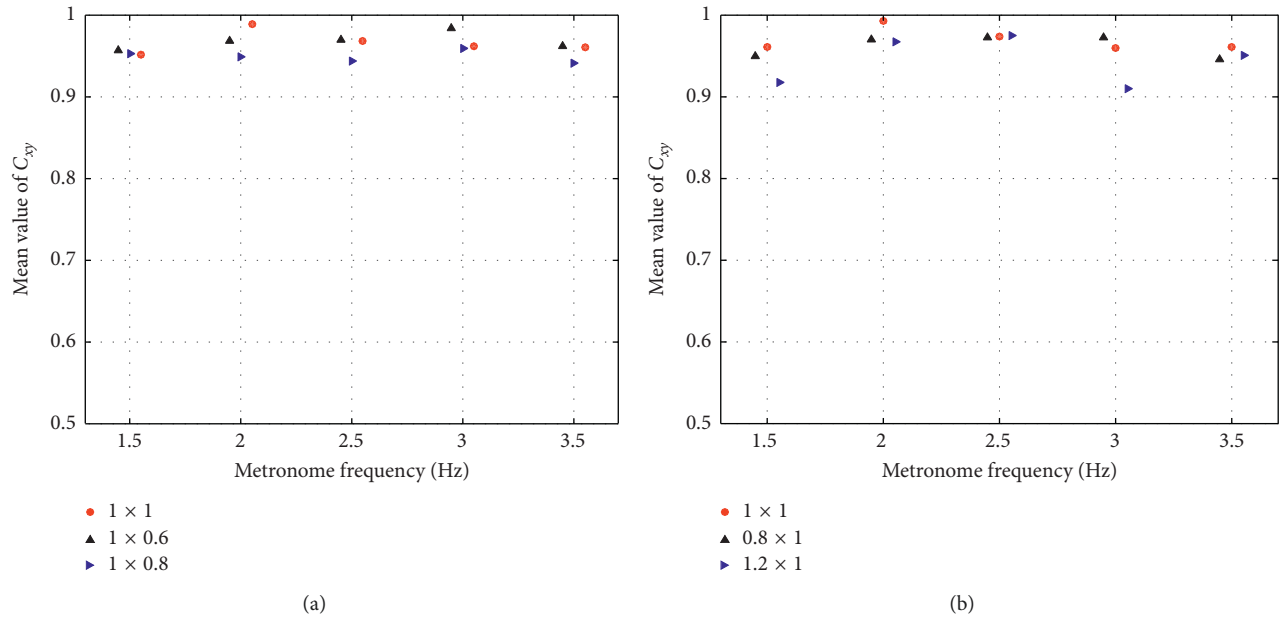

Figure 30: Comparison of the mean values of the coherence coefficient with a single distance in two groups. (a) Group 01; (b) group 02.

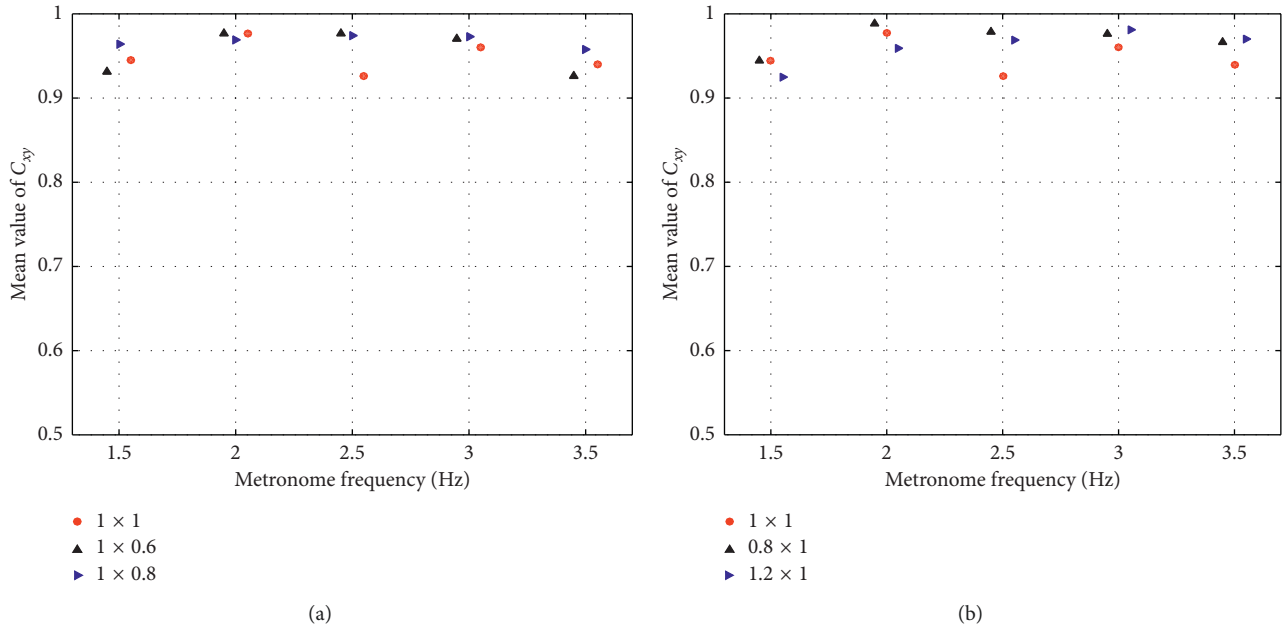

Figure 31: Comparison of the mean values of coherence coefficients with double distances in two groups. (a) Group 01; (b) group 02.

experimental data, and the situation with an eyepatch is too extreme to happen in reality, so we do not need to account for it.

4.3. Influence of Auditory Stimuli. To investigate the influence of auditory stimuli, the experiments considered both a metronome cue and music songs. In total, 11 songs are considered in the experimental study, including eight English songs, two Chinese songs, and a single Japanese song for the reference configuration. The dominant tempos of the songs are 1.50, 1.57, 1.75, 1.83, 2.0, 2.08, 2.3, 2.37, 2.5, and 2.73 Hz. The corresponding metronome frequencies involve 1.5, 1.6, 1.7, 1.8, 2.0, 2.1, 2.3, 2.4, 2.5, and 2.7 Hz.

4.3.1. Normalized Achieved Bouncing Frequency and Equivalent Bandwidth. Figure 38 shows the comparison of the normalized achieved bouncing frequency for cases with metronome compared to the tempo based on metronome measurement of songs played during testing. Figure 38 presents the corresponding equivalent bandwidth. For the case where a metronome cue is used, the normalized achieved frequency is close to unity. When a song is used,

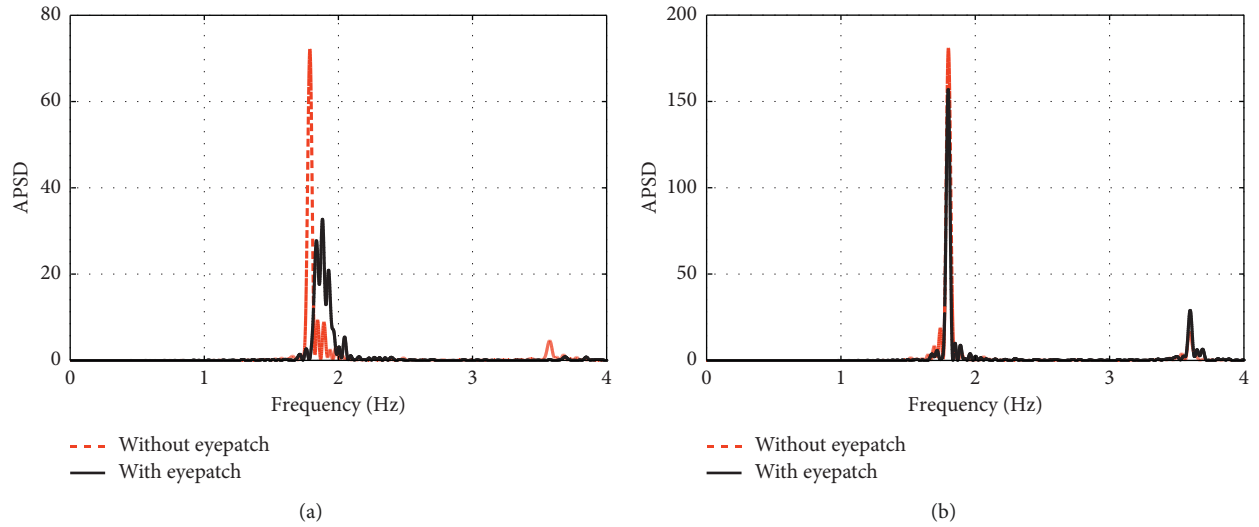

Figure 32: PSDs of the clavicle acceleration of (a) Participant No. 32 and (b) Participant No. 13 bouncing with and without an eyepatch for the 1×1 m configuration at 1.8 Hz.

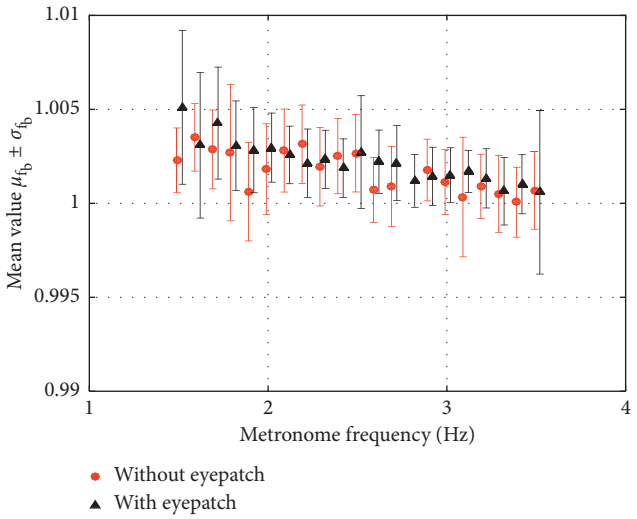

Figure 33: Comparison of the normalized achieved bouncing frequency for visual stimuli, with and without an eyepatch.

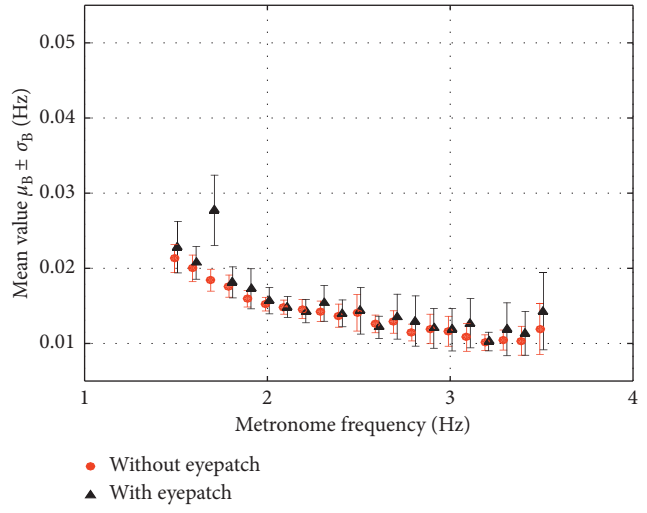

Figure 34: Comparison of the equivalent bandwidth for visual stimuli, with and without an eyepatch.

the standard deviation from the rhythm of the auditory stimuli is much larger, especially for the songs with a metronome tempo of 1.53, 1.75, 1.83, and 2.3 Hz. In turn, Figure 39 shows that the equivalent bandwidth is much larger when a song is applied compared to metronome-only results.

These results indicate that it is much easier for participants to follow the metronome cue. The metronome performance is also more consistent when analyzing the correlation and coordination.

4.3.2. Time Lag and Coordination Factor. Figures 40(a) and 40(b) compare the time lags and the correlation values for the metronome cases and the song cases. Figure 41 presents the results of the coordination factors for the auditory stimuli—the metronome and music. From Figures 40 and 41, it is clear that the correlation values and the coordination factors when participants are listening to a song are much lower than those when a metronome cue is used.

The results indicate that higher levels of synchronization are attained when the auditory cue is the metronome in comparison to the tempo of music based on participants listening to different songs during the bouncing sessions.

5. Conclusions

This study experimentally investigates the individual and global bouncing motion. First, small-scale laboratory experiments involving the simultaneous registration of the body motion and the resulting GRFs are applied to show

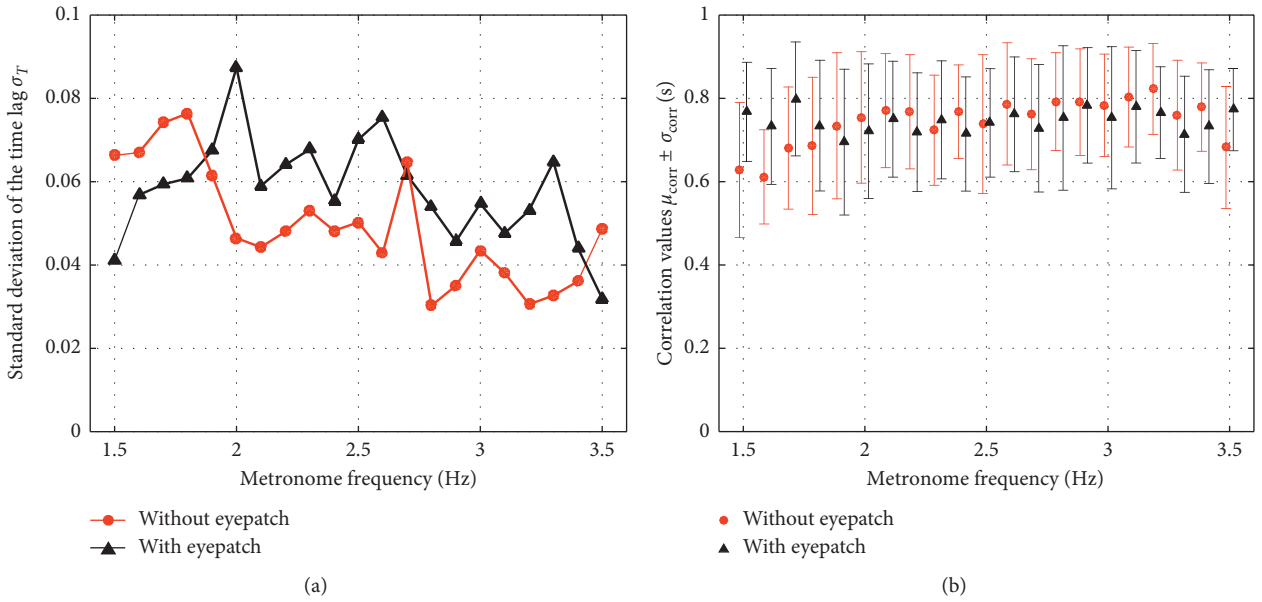

Figure 35: Comparison of the time lags (a) and correlation values (b) for visual stimuli, with and without an eyepatch.

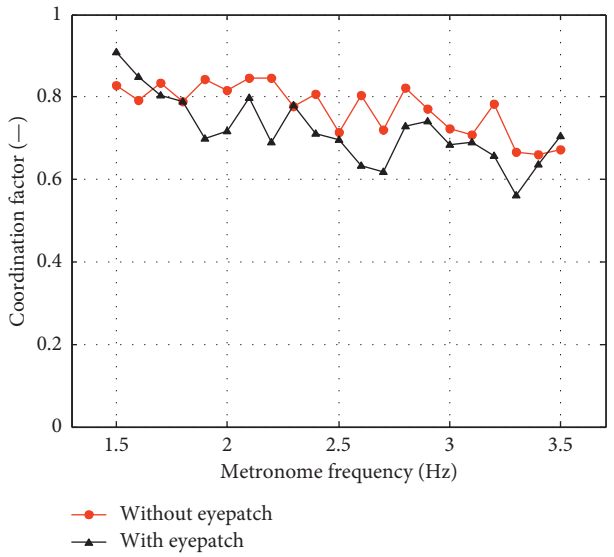

Figure 36: Comparison of the coordination factors for visual stimuli, with and without an eyepatch.

how the trajectory of the clavicle can be used to qualitatively represent the bouncing motion of a person and also to analyze the synchronization between bouncing persons. Second, a full-scale experimental study was performed where the bouncing motion of 48 persons was simultaneously recorded and 330 test cases were performed. The intra- and interperson variability in the fundamental bouncing frequency and the level of synchronization in the crowd are investigated for a realistic range of bouncing frequencies (from 1.5 Hz to 3.5 Hz with an interval of 0.1 Hz). Furthermore, the influence of various stimuli (spatial, visual, and auditory stimuli) is investigated.

The results show that the lowest degree of inter- and intraperson variability in the fundamental bouncing frequency is found when recorded metronome rhythms range between 2.6 Hz and 3.4 Hz, showing that, for individuals, these rhythms are the easiest to follow. However, during these higher frequencies, participants pay more attention to their own movements instead of noticing the motions of other participants. Thus, these ranges are characterized by the lowest level of synchronization. In turn, the analysis of the lateral and frontal coherence shows that coherence coefficients at frequencies between 2.6 Hz and 3.4 Hz are more dispersive.

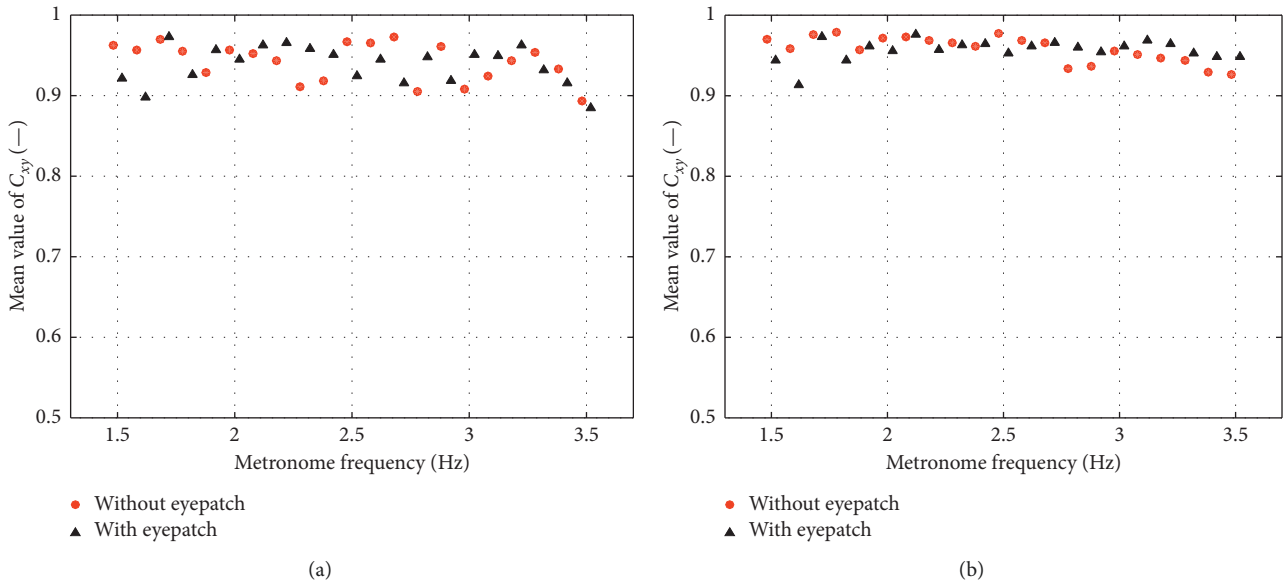

Figure 37: Comparison of the mean values of the (a) lateral coherence coefficients and (b) frontal coherence coefficients for visual stimuli, with and without an eyepatch.

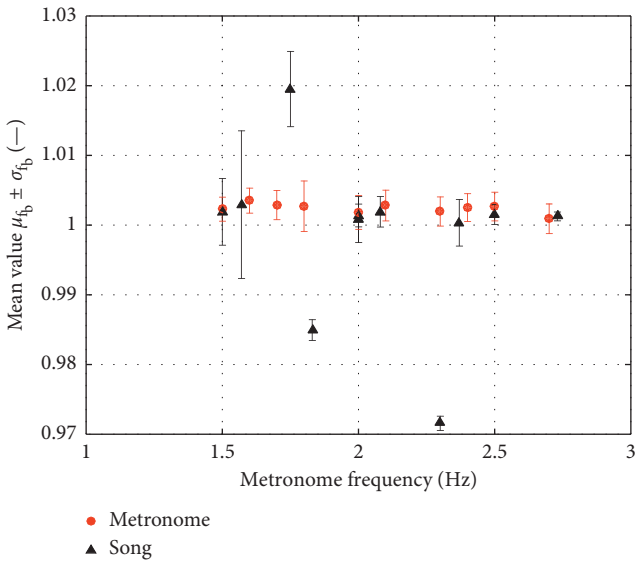

Figure 38: Comparison of the normalized achieved bouncing frequency for auditory stimuli.

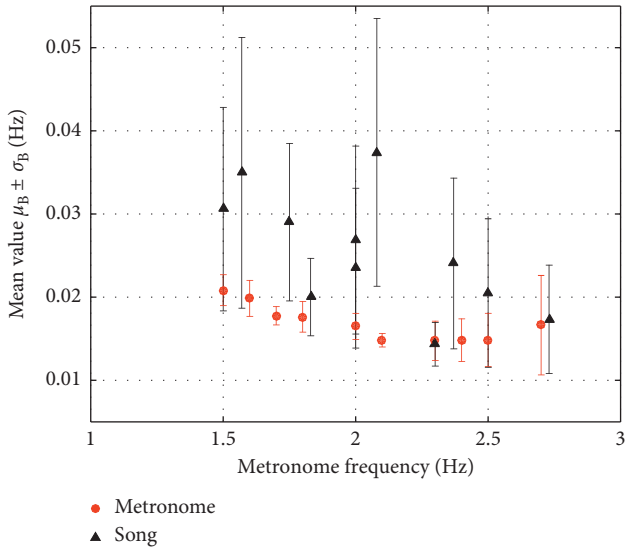

Figure 39: Comparison of the equivalent bandwidth for auditory stimuli.

Different spatial configurations are considered, ranging from 0.6 m to 1.2 m. Apart from the coordination factor which (slightly) increases with decreasing frontal distance (0.8 m and 1.2 m), no relevant impact on the inter- and intraperson variability in the bouncing motion or in the overall crowd behavior is observed for the considered spatial configurations. The reason might be that the range of spacing was too small to present some certain tendency.

The impact of visual stimuli is investigated by using an eyepatch on each participant. It is observed that the elimination of the visual connection will lower individual bouncing consistency, which is assumed to be due to the uncertainty-limited vision that can make participants focus on their own bouncing behavior. In addition, correlation values and coordination factors are also lower for participants tested wearing eyepatches. In addition to tests where a metronome cue was used, 10 songs with different rhythms were also involved. The results indicate that significantly higher levels of synchronization and a lower degree of the intraperson variability are attained with a metronome cue compared to the beat of songs.

The results in this paper were obtained from the crowd standing on a rigid ground. Hence, these conclusions may be more suitable for rather stiff structures

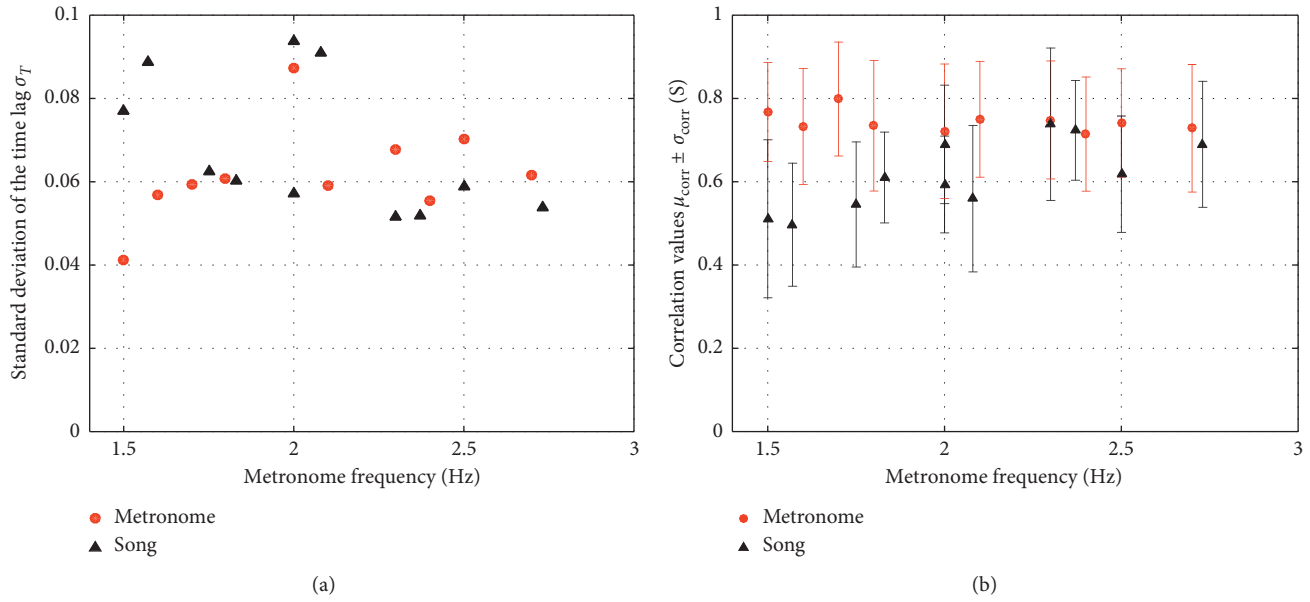

Figure 40: Comparison of the time lags (a) and correlation values (b) for auditory stimuli metronome and songs.

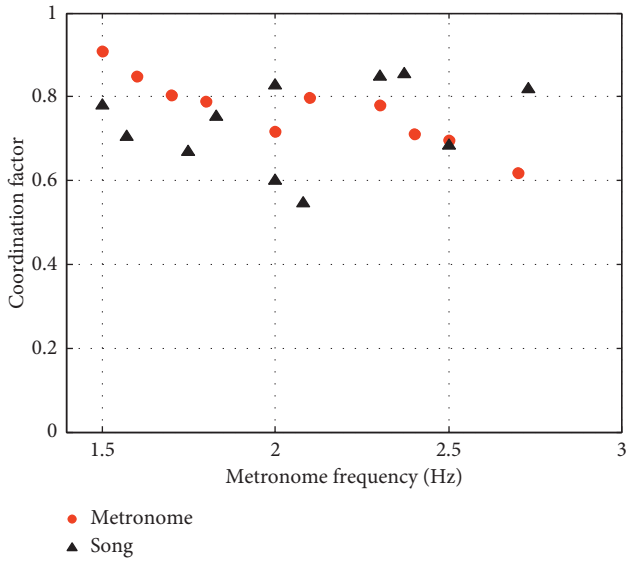

Figure 41: Comparison of the coordination factors for auditory stimuli—metronome and song.

than slender structures sensitive to human-induced vibrations. That is, the effect of human-structure interaction on the synchronization behavior of the crowd is not accounted for.

Data Availability

The experimental result data used to support the findings of this study have not been made available because further study based on these data has not been published.

Conflicts of Interest

The authors declare that they have no conflicts of interest.

Acknowledgments

Financial support for this research was awarded to the corresponding author from the National Natural Science Foundation (51478346), State Key Laboratory for Disaster Reduction of Civil Engineering (SLDRCE14-B-16), and Xinjiang University through Tianshan Talent Program. The authors would like to thank all those who participated in this experiment.

References

[1] C. A. Jones, P. Reynolds, and A. Pavic, "Vibration serviceability of stadia structures subjected to dynamic crowd loads: a literature review," *Journal of Sound and Vibration*, vol. 330, no. 8, pp. 1531–1566, 2011.

[2] Standing Committee on Structural Safety, *Structural Safety 2000-01: 13th Report of SCOSS*, pp. 23-24, Standing Committee on Structural Safety, London, UK, 2001.

[3] J. G. Parkhouse and D. J. Ewins, "Crowd-induced rhythmic loading," *Proceedings of the Institution of Civil Engineers—Structures and Buildings*, vol. 159, no. 5, pp. 247–259, 2006.

[4] J. L. Chen, R. J. Zatorre, and V. B. Penhune, "Interactions between auditory and dorsal premotor cortex during synchronization to musical rhythms," *NeuroImage*, vol. 32, no. 4, pp. 1771–1781, 2006.

[5] E. Duarte and T. Ji, "Action of individual bouncing on structures," *Journal of Structural Engineering*, vol. 135, no. 7, pp. 818–827, 2009.

[6] Danish Code (DS410), *Code of Practice for Loads for the Design of Structures*, Danish Standards, Copenhagen, Denmark, 1998.

[7] V. Racic and J. Chen, "Data-driven generator of stochastic dynamic loading due to people bouncing," *Computers & Structures*, vol. 158, pp. 240–250, 2015.

[8] J. Chen, L. Wang, V. Racic, and J. Lou, "Acceleration response spectrum for prediction of structural vibration due to

individual bouncing," *Mechanical Systems and Signal Processing*, vol. 76-77, pp. 394–408, 2016.

[9] S. E. Mouring, "Dynamic response of floor systems to building occupant activities," Ph.D. Dissertation, Johns Hopkins University, Baltimore, MD, USA, 1992.

[10] J. M. W. Brownjohn, A. Pavic, and P. Omenzetter, "A spectral density approach for modelling continuous vertical forces on pedestrian structures due to walking," *Canadian Journal of Civil Engineering*, vol. 31, no. 1, pp. 65–77, 2004.

[11] R. Vitomir, J. M. W. Brownjohn, and A. Pavic, "Dynamic loads due to synchronous rhythmic activities of groups and crowds," in *Proceedings of the COMPDYN 2011-3rd International Conference on Computational Methods in Structural Dynamics and Earthquake Engineering*, Corfu, Greece, May 2011.

[12] N. Noormohammadi, J. Brownjohn, A. Wing et al., "Effect of different cues on spectators' synchronisation a vibration engineering approach," in *Proceedings of the 8th International Conference on Structural Dynamics*, Leuven, Belgium, July 2011.

[13] R. Vitomir, J. M. Brownjohn, S. Wang, M. T. Elliot, and A. Wing, "Effect of sensory stimuli on dynamic loading induced by people bouncing," in *Topics in Dynamics of Civil Structures*, vol. 4, pp. 365–369, Springer, New York, USA, 2013.

[14] L. Georgiou, V. Racic, J. M. Brownjohn, and M. T. Elliot, "Coordination of groups jumping to popular music beats," in *Dynamics of Civil Structures*, vol. 2, pp. 283–288, Springer International Publishing, Berlin, Germany, 2015.

[15] A. J. Comer, A. Blakeborough, and M. S. Williams, "Rhythmic crowd bobbing on a grandstand simulator," *Journal of Sound and Vibration*, vol. 332, no. 2, pp. 442–454, 2013.

[16] T. Ji and B. R. Ellis, "Human-structure interaction in vertical vibrations," *Proceedings of the Institution of Civil Engineers—Structures and Buildings*, vol. 122, pp. 1–9, 1997.

[17] A. Cappellini, S. Manzoni, and M. Vanali, "Quantification of damping effect of humans on lightly damped staircases," *Topics in Dynamics of Civil Structures,*vol. 4, pp. 453–460, 2013.

[18] K. A. Salyards and N. C. Noss, "Experimental evaluation of the influence of human-structure interaction for vibration serviceability," *Journal of Performance of Constructed Facilities*, vol. 28, no. 3, pp. 458–465, 2014.

[19] L. Wang, J. Chen, and Y. X. Peng, "Novel techniques for human-induced loading experiment and data processing," in *Proceeding of the International Symposium on Innovation & Sustainability of Structures in Civil Engineering*, Xiamen, China, October 2011.

[20] J. G. Richards, "The measurement of human motion: a comparison of commercially available systems," *Human movement science*, vol. 18, no. 5, pp. 589–602, 1999.

[21] K. Van Nimmen, G. Lombaert, G. De Roeck, and P. Van den Broeck, "Simulation of human-induced vibrations based on the characterized in-field pedestrian behavior," *Journal of Visualized Experiments*, vol. 110, article e53668, 2016.

[22] A. Cappozzo, U. Dellacroce, A. Leardini, and L. Chiari, "Human movement analysis using stereophotogrammetry. part 1: theoretical background," *Gait & Posture*, vol. 21, no. 2, pp. 186–196, 2005.

[23] M. S. Zhang, J. Chen, Y. X. Peng, and L. Wang, "Reproduction and simulation of walking induced load via motion capture technique and inverse dynamics of rigid body models," *Journal of Engineering Science*, vol. 21, no. 5, pp. 961–972, 2013, in Chinese.

[24] Y. Peng, J. Chen, and G. Ding, "Walking load model for single footfall trace in three dimensions based on gait experiment," *Structural Engineering and Mechanics*, vol. 54, no. 5, pp. 937–953, 2015.

[25] F. T. da Silva, H. M. B. F. Brito, and R. L. Pimentel, "Modeling of crowd load in vertical direction using biodynamic model for pedestrians crossing footbridges," *Canadian Journal of Civil Engineering*, vol. 40, no. 12, pp. 1196–1204, 2013.

[26] K. Van Nimmen, G. Zhao, A. Seyfarth, and P. Van den Broeck, "A robust methodology for the reconstruction of the vertical pedestrian-induced load from the registered body motion," *Vibration*, vol. 1, no. 2, pp. 250–268, 2018.

[27] J. Chen, H. Tan, and Z. Pan, "Experimental validation of smartphones for measuring human-induced loads," *Smart Structures and Systems*, vol. 18, no. 3, pp. 625–642, 2016.

[28] Z. Pan and J. Chen, "Measurements of pedestrian's load using smartphones," *Structural Engineering and Mechanics*, vol. 63, no. 6, pp. 771–777, 2017.

[29] Mathworks, *Global Optimization Toolbox: User's Guide (r2016b)*, Mathworks, Natick, MA, USA, 2016, http://www.mathworks.com/help/pdf_doc/gads/gads_tb.pdf.

[30] B. Iglewicz and D. Hoaglin, "Volume 16: how to detect and handle outliers," in *The ASQC Basic References in Quality Control: Statistical Techniques*, E. F. Mykytka, Ed., American Society for Quality Control, Milwaukee, WI, USA, 1993.

[31] J. Chen, J. Wang, and J. M. Brownjohn, "Power spectral-density model for pedestrian walking load," *Journal of Structural Engineering*, vol. 145, no. 2, article 04018239, 2019.

[32] P.-E. Eriksson, *Vibration of Low-Frequency Floors-Dynamic Forces and Response Prediction*, Chalmers University of Technology, Gothenburg, Sweden, 1994.

[33] V. Racic, A. Pavic, and J. M. W. Brownjohn, "Experimental identification and analytical modelling of human walking forces: literature review," *Journal of Sound and Vibration*, vol. 326, no. 1-2, pp. 1–49, 2009.

[34] T. J. Karras, *Equivalent Noise Bandwidth Analysis from Transfer Functions*, National Institute of Standards and Technology, Gaithersburg, MD, USA, 1965.

[35] A. Shapiro, "Monte Carlo sampling methods," *Handbooks in Operations Research and Management Science 10*, pp. 353–425, Elsevier, Amsterdam, Netherlands, 2003.

[36] S. Emil and R. H. Scanlan, *Wind Effects on Structures: Fundamentals and Application to Design*, John Willey & Sons Inc., Hoboken, NJ, USA, 1996.